

1 **GPR signature of Quaternary faulting: A study from the Mt. Pollino**
2 **region, southern Apennines, Italy.**

3 Maurizio Ercoli¹⁻⁴, Daniele Cirillo²⁻⁴, Cristina Pauselli¹⁻⁴, Harry M. Jol³, Francesco Brozzetti²⁻⁴

4 ¹: Università degli Studi di Perugia, Dipartimento di Fisica e Geologia, Piazza dell'Università 1, 06123 Perugia,
5 Italy.

6 ²: Università "G. d'Annunzio" di Chieti-Pescara, DiSPUTer, via dei Vestini 31, 66100 Chieti, Italy.

7 ³: University of Wisconsin - Eau Claire, Department of Geography and Anthropology, 105 Garfield Avenue, Eau
8 Claire, WI, 54702.

9 ⁴: CRUST Centro interUniversitario per l'analisi SismoTettonica tridimensionale, Italy.

11 Correspondence to: Maurizio Ercoli (maurizio.ercoli@unipg.it; maurizio.ercoli@gmail.com)

12 **Abstract.** With the aim of unveiling evidence of Late Quaternary faulting, a series of ground penetrating radar (GPR)
13 profiles were acquired across the southern portion of the Fosso della Valle-Campotenesse normal fault (VCT) located
14 at the Campotenesse continental basin (Mt. Pollino region), in the southern Apennines active extensional belt (Italy).
15 A set of forty-nine 300 MHz and 500 MHz GPR profiles, traced nearly perpendicular to this normal fault, were
16 acquired and carefully processed through a customized workflow. The data interpretation allowed us to reconstruct a
17 pseudo-3D model depicting the boundary between the Mesozoic bedrock and the sedimentary fill of the basin, which
18 were in close proximity to the fault. Once reviewing and defining the GPR signature of faulting, we interpret near-
19 surface alluvial and colluvial sediments dislocated by a set of conjugate (W- and E-dipping) discontinuities that
20 penetrate inside the underlying Triassic dolostones. Close to the contact between the continental deposits and the
21 bedrock, some buried scarps which offset wedge-shaped deposits are interpreted as coseismic ruptures, subsequently
22 sealed by later deposits. Although the use of pseudo-3D GPR data implies more complexity linking the geophysical
23 features among the radar images, we have reconstructed a reliable subsurface fault pattern, discriminating master
24 faults and a series of secondary splays. We believe our contribution provides an improvement in the characterization
25 of active faults in the study area which falls within the Pollino seismic gap and is considered potentially prone to
26 severe surface faulting. Our aim is for our approach and workflow to be of inspiration for further research in the study
27 site, as well as for similar high seismic hazard regions characterized by scarcity of near-surface geophysical data.

29 **Key-words:** ground penetrating radar (GPR); Image processing; Faults; Neotectonics; Palaeoseismology;
30 Earthquake hazards.

31 **1. Introduction**

32 A "seismic gap" is an area surrounded by regions struck by large earthquakes in historical or recent times. Such
33 earthquake-free areas are characterized by the presence of seismogenic faults, whose past activity or possible
34 quiescence is inferred on the basis of morpho-structural and/or paleoseismological data. The "seismic gaps" (McCann
35 et al., 1979) show an apparent lack of historical seismicity but are candidate regions for the occurrence of large
36 earthquakes in the near future (Mogi 1979; Plafker and Galloway 1989; Cinti et al., 1997; Galadini and Galli, 2003).
37 A recent example of a seismic gap, "filled" by strong earthquakes is the Mt. Vettore area (central Apennines) during
38 the 2016-2017 seismic sequence (Chiaraluce et al., 2017; Barchi et al., 2021 and references therein). Following the

Deleted: a

Deleted: G

Deleted: P

Deleted: R

Deleted: the

Deleted: a

Deleted: sector

Deleted: a buried

Deleted: highlight

Deleted: in our data how

Deleted:

Deleted: appear to be

Deleted: west

Deleted: east

Deleted: studies

Deleted: he

Deleted: region

Deleted: areas

Deleted: of surface geological information but

Deleted: G

Deleted: P

Deleted: R

Deleted: region

Deleted: It

Deleted: is

Deleted: active

Deleted: active

Deleted:

Deleted: ich

Deleted: ,

Deleted: , that are evaluated seismically "silent" during the
historical or recent times

Deleted: record (Galadini and Galli 2003), but which are
considered, on the basis of paleoseismological

Deleted: Such

Deleted: are and/or morpho-structural data,

Deleted: able to generate significant

Deleted: McCann et al. 1979;

Deleted: Although the hypothesis stating that the earthquake
potential increases after a long quiet period was rejected by [...]

Deleted: Structural and geomorphological evidence may [...]

Deleted: As shown by

Deleted: seismic sequence in central Apennines

Deleted: Mw = 6.5 "Norcia" mainshock,

Deleted: ,

Deleted:

extensive coseismic ruptures mainly generated by the $M_w = 6.5$ “Norcia” mainshock (Villani et al., 2018; Brozzetti et al., 2019; Testa et al., 2019), this area is currently an ideal laboratory for many conventional and innovative geoscience disciplines and applications (e.g. Xu et al., 2017; Porreca et al., 2018; Brozzetti et al., 2020; Cirillo, 2020; Ferrario et al., 2018; Ercoli et al., 2020; Michele et al., 2020; Porreca et al., 2020; Buttinelli et al., 2021; Ferrarini et al., 2021; Pucci et al., 2021; Sapia et al., 2021; Villani et al., 2021). In fact, although the area being characterized by a complex alignment of normal faults, no important earthquakes were reported over the past ~1500 years before this seismic crisis (Cinti et al., 2019; Galli et al., 2019; Galli, 2020). Former geological and geomorphological studies suggested the possible occurrence of Quaternary faulting (Calamita et al., 1992; Brozzetti and Lavecchia 1994; Barchi et al., 2000), which was successively confirmed by paleoseismological (Galadini and Galli, 2003) and GPR surveying (Ercoli et al., 2013a; 2014). These studies revealed the occurrence of strong paleo-earthquakes and suggested that the Mt. Vettore master fault was “silent”, but prone to cause future seismic events. However, invasive trenching due to complex logistics, environmental restrictions, high costs and the need for authorizations, cannot be applied systematically in many locations. Thus, Quaternary faults and associated basins characterized by an unsatisfactory definition of the seismotectonic framework have to be investigated with geophysical techniques. For all the above noted reasons, and since the Mt. Vettore case may represent an analogue of similar seismic gaps, the southernmost Apennines were studied through a dedicated research programme (Agreement INGV-DPC 2012-2013 and 2014-2015, Project S1 - Base-knowledge improvement for assessing the seismogenic potential of Italy, Brozzetti et al., 2015; Pauselli et al., 2015) aiming to improve the knowledge-base of seismogenic structures. In the research, focused also on the Calabrian region (Southern Italy), during the 2012-2015 period, structural geology, geophysical, and paleoseismological data were successfully acquired on the Mt. Pollino and Castrovillari fault systems (northern Calabria), providing evidence of Late Quaternary activity (Ercoli et al., 2013b; Cinti et al., 2015; Ercoli et al., 2015; Brozzetti et al., 2017b). This area, which is considered one of the most important seismic gaps in southern Italy, extends from the Mercure basin to the north until Campotenese basin and Castrovillari plain to the south, all characterized by Late Quaternary continental syn-tectonic sedimentation (Fig. 1a-c). The paleoseismological trenching and radiocarbon dating document in the region the occurrence of paleo-earthquakes with $6.5 < M_w < 7.0$ and a recurrence time interval of ~1200 years (Cinti et al., 1997, 2002, 2015a,b; Michetti et al., 1997, 2000). But this high magnitude interval contrasts with the historical seismicity records, reporting a single significant $M_w 5.2$ event occurred in 1693 (Tertulliani and Cucci, 2014). In the last three decades instrumental seismicity recorded only two moderate seismic sequences climaxed in the $M_w 5.6$ Mercure (1998, September 9) and $M_w 5.2$ Mormanno (2012, October 25) earthquakes. The latter occurred during a long-lasting sequence spanning the period 2010-2014, which included more than 6000 seismic events of $M_w > 1$ and activated at least three individual seismogenic sources (Passarelli et al., 2015; Brozzetti et al., 2017a; Fig. 1b). The gap between the low energy release, observed during the instrumented seismic sequences, and the high seismic potential estimated for the Quaternary faults, raised the question of whether even stronger earthquakes had shaken and could shake the area in the future. A recent and detailed parameterization of the Fosso della Valle-Campotenese fault (VCT in Fig. 1c), based on geo-structural and geomorphological mapping (Brozzetti et al., 2017a) as well as on seismological evidence (Totaro et al., 2014, 2015; Cirillo et al., 2021), assesses a surface length of 15 km and a depth of at least ~10 km; the potential rupture-area is likely estimated to produce $M_w > 6.0$ earthquakes. As testified by earthquakes of the last century, such magnitudes, in the Apennines extensional belt, generally produce coseismic surface faulting (e.g. Oddone, 1915; Pantosti and Valensise, 1990; Boncio et al., 2010; Brozzetti et al., 2019). However, Quaternary faulting for the VCT,

Deleted: ...o important earthquakes were reported over the past ~1500 years before this seismic crisis (Cinti et al., 2019; Galli et al., 2019; Galli, 2020) displaced characterized by ... Former an alignment a complex set of west-dipping Quaternary faults (Ercoli et al., 2020) which, produced extensive coseismic break surface faulting (Villani et al. 2018 and references therein; Brozzetti et al. 2019; Testa et al. 2019), where no important earthquakes had been recorded over the past 1500 years. Nine-strong and moderate seismic events struck a ~80 km long region, climaxing in the $M_w = 6.5$ “Norcia” mainshock (Porreca et al. 2018 and references therein; Ercoli et al. 2020), producing extensive surface faulting (Pucci et al. 2017; Civico et al. 2018; Villani et al. 2018; Brozzetti et al. 2019, 2020; Testa et al. 2019; Cirillo 2020). ... Geological and geomorphological and

Moved (insertion) [1]

Deleted: studies ...urveying (across the faults set were preceding this seismic sequence (Calamita et al. 1992; ...

Moved up [1]: Calamita et al. 1992; Brozzetti and

Deleted: detected a peculiar geophysical signature

Deleted: , that was not very prominent on the present

Deleted: led to consider...uggested that the Mt. Vettore

Deleted: similar strong

Deleted: Such an experience in the future. Thise proves

Deleted: of the Apennines

Deleted: .

Deleted: Its systematic application may provide answers

Deleted: But on many active faults, contrary to geophysic

Deleted: paleoseismological data

Deleted: techniques (e.g. ...renching) cannot be carried

Deleted:

Deleted: A... dedicated research project

Deleted: base-...nowledge- ...ase of seismogenic structur

Deleted: studies ...ata were successfully acquired across

Deleted: supporting

Deleted: their

Deleted: extends northward to include the Mercure and

Deleted: The fresh geomorphic signature of the faults

Deleted: 6

Deleted: 2...event occurred in 1693 (Guidoboni et al.

Deleted:

Deleted: n...based on geo-structural and geomorphologica

Deleted: (Brozzetti et al. 2017a; Cirillo et al., 2021)

Deleted: $M_w >$

Deleted: Such seismic events... in the Apennines

Deleted: , E.

Deleted: Valensise

Deleted: ; Cello et al. 2000; Vittori et al. 2000

Deleted: Villani et al. 2018;

Deleted: evidence of ...uaternary faulting for the VCTis

1 structure is currently unclear, but geological and morpho-structural data suggest this fault has played an important role
 2 in determining the geometry and the recent sedimentary evolution of the basin.
 3 The Campotenese basin and its VCT boundary fault is an example that summarizes the aforementioned issues: 1) lack
 4 of availability of paleoseismological data as the basin is entirely located within the Mt. Pollino National Park, thus
 5 requiring prior authorization from authorities; 2) lack of availability of publically accessible geophysical data; 3) no
 6 fresh recent surface displacements within the Holocene deposits have been observed along its trace. For all these
 7 reasons, the VCT represents an ideal case study suitable to test our working method.
 8 We have conducted an explorative GPR field campaign across a VCT sector, suggested by discontinuous and smooth
 9 geomorphic scarps, as a screening tool for the definition of its possible Quaternary displacement history. The
 10 objectives of the paper are to: i) review and describe geophysical characteristics associated with a peculiar GPR
 11 signature of faulting, and propose a reference methodological workflow; ii) specifically check the efficiency of GPR
 12 prospecting to locate the VCT fault and to depict its subsurface pattern and spatial continuity at shallow depth; iii)
 13 provide new data to eventually relate the occurrence of $M_w > 6.0$ seismic events; iv) pave the way for other local
 14 geophysical studies and identify interesting sites for future ground-truthing and/or paleoseismological trenching; v) to
 15 have direct application and impact to the planning of future mitigation strategies for the reduction of surface faulting
 16 risk in the nearby urbanized areas.

17 2. Tectonic setting and seismicity

18 The Campotenese continental basin is located in the northernmost Calabria region south-west of the Mt. Pollino
 19 calcareous massif (southern Italy, Fig. 1). The bedrock of the basin consists of shallow water dolostones and
 20 limestones, Late Triassic to Middle Miocene in age, belonging to the Verbicaro tectonic unit (Ogniben, 1969; Amodio
 21 Morelli et al., 1976). It is generally referred to the western edge of the “Apenninic Platform”, a thick (> 4 km)
 22 carbonate shelf, that underwent compression during the Middle-Late Miocene times and was translated over an eastern
 23 basinal domain (Lagronegro-Molise basin; Patacca and Scandone, 2007; Vezzani et al., 2010 and references therein).
 24 From the bottom to the top, the bedrock succession includes late Triassic dolostones, Cretaceous limestones, and
 25 Paleocene-Lower Miocene calcarenites cross-cut by the pillow lava basalts belonging to Liguride units of the
 26 northern sector of Calabrian arc (Quitow, 1935, Grandjaquet and Grandjaquet, 1962, Amodio Morelli et al., 1976,
 27 Ghisetti and Vezzani, 1983; Iannace et al., 2004, 2005 and 2007; Liberi et al., 2006; Filice et al., 2015 and Tangari et
 28 al., 2018).

29 The origin of the Campotenese basin, however, is related to a set of NW-SE striking extensional faults which, during
 30 the Middle-Late Pleistocene, displaced the contractional tectonic pile, favoring the deposition of alluvial and lacustrine
 31 sediments in a subsiding intra-mountain depression (Servizio Geologico d'Italia 1970). This set of conjugate SW- and
 32 NE-dipping normal faults represents the local expression of the Quaternary extensional belt that develops all along
 33 the Italian peninsula, nearly parallel to the axial zone of the Apennines, from northern Tuscany to the Calabrian Arc
 34 (Brozzetti 2011). North of Campotenese, (Lucania and southern Campania) the Apennine extensional belt includes
 35 several continental basins and their boundary faults, as the Irpinia, Vallo di Diano, Tanagro, Melandro-Pergola and
 36 Val d'Agri (Ascione et al., 1992; Maschio et al., 2005; Amicucci et al., 2008; Villani and Pierdominici, 2010;
 37 Brozzetti, 2011; Filice and Seeber, 2019 and Bello et al., 2021). To the south, it continues with the Crati graben that
 38 dissects the northern sector of the Calabrian Arc (Tortorici et al., 1995; Brozzetti et al., 2017b).

Deleted: !

Deleted:

Deleted: emblematic

Deleted: un

Deleted: competent

Deleted: un

Deleted: no

Deleted: evidence of

Deleted: of

Deleted: , suggesting the occurrence of recent strong earthquakes,...

Deleted: so far

Deleted: in recent times

Deleted: ¶

Deleted: , as it

Deleted: we

Deleted: the detections of potential unknown Quaternary co-seismic ruptures along its fault zone

Deleted: It is possible that, during past strong earthquakes, propagation of coseismic ruptures along the fault could have displaced Holocene deposits at the surface, being subsequently buried by further and more recent alluvial deposits or erased by the anthropogenic and agricultural activity,...

Deleted: project

Deleted: GPR

Deleted:

Deleted: for the study site which might be extended to other areasto use

Deleted: to use in similar studies

Deleted: a

Deleted: prospection

Deleted: specifically in the Campotenese study site

Deleted: trace of the

Deleted: studied

Deleted: as well as

Deleted: verify

Deleted: ing

Deleted: to

Deleted: on the VCT, as observed for the nearby Castrovillari faults; iv) highlight new elements for more exhaustive characterization of the VCT

Deleted: with the purpose of better

Deleted: and quantification of its seismogenic potential

Deleted: prospections

Deleted: i

On the regional scale, the Quaternary normal fault array controls the release of major seismicity, as suggested by the distribution of supra-crustal instrumental earthquakes (INGV, 2020 and JSIDe, 2007) and of the strongest historical events (Fig. 1a, Tertulliani and Cucci, 2014; Rovida et al., 2020). The recent seismic activity as well as paleo-seismological investigations claim that most of the faults bounding the Quaternary basins are seismogenic and therefore enable, in some cases, to associate major past earthquakes with specific structures (e.g. Pantosti and Valensise, 1990; Cello et al., 2003; Spina et al., 2009; Brozzetti et al., 2009; Villani and Pierdominici, 2010). These same studies highlight that the kinematics of the Quaternary faults and the focal mechanisms of the major earthquakes are mutually consistent and are mainly compatible with an SW-NE direction of extension (RCMT and TDMT databases by Pondrelli, 2006 and Scogliamiglio et al., 2006). Other authors have recognized in the surrounding regions an oblique normal-lateral faults kinematics (e.g. Rossano and Sybaris faults, Galadini et al., 2001 and Cinti et al., 2015b).

The fault investigated in this work has been pointed out in more detail by Brozzetti et al. (2017a), in the frame of a larger study focussed on the Quaternary and active faults at the Calabrian-Lucanian boundary (Fig. 1a). In the region, three main sets of normal faults, with prevailing dip-slip kinematics, have been mapped: a western one, consisting of E- to NNE-dipping faults (red lines in Fig. 1b), and two other main sets of W- to SW-dipping fault segments (dark-blue and blue lines in Fig. 1b). The Rotonda-Campotenese Set (ROCS) is a right-stepping en-échelon master fault developed for a total length of 15 km with an average N160E strike (blue, yellow rimmed lines in Fig. 1b). ROCS is composed by two fault segments: i) the westernmost Fosso della Valle-Campotenese fault (VCT), which extends from the southern border of the Mercure basin to the SW boundary of the Campotenese basin, and ii) the Rotonda-Sambucoso fault (RSB), which branches-out from the VCT segment in the central part of the ROCS. In the northern sector, the two segments are averagely spaced ~ 2.5 km at surface and linked at a depth of ~ 9-10 km (Cirillo et al., 2021), cross-cutting the middle-Pleistocene ~ E-W striking Cozzo Vardo-Cozzo Nisco fault (CVN, light-blue line in Fig. 1b). Along the E-side of the Campotenese basin, the VCT is generally buried by Holocene deposits, but its location can be inferred based on stratigraphic observations and geomorphic features, such as sharp ridge fronts, linear scarps, and slope breaks. The VCT controls the distribution and thickness of the clastic fill basin (Middle Pleistocene-Holocene in age, according to Schiattarella et al., 1994) that reaches the maximum thickness (~30 m) in the western sector (VCT hanging wall, see boreholes stratigraphy at <http://sgi2.isprambiente.it/mapviewer/>). The spatial relationships, at surface and depth, between the Quaternary fault segments and the hypocenters of the re-located 2010-2014 seismic events (Totaro et al., 2015; Brozzetti et al., 2017a; Napolitano et al., 2020, 2021; Pastori et al., 2021) suggest that the VCT is a good candidate as a seismogenic source for the Mw 5.2 (2012, October 25) Mormanno earthquake, as well as for strong paleo-events.

FIGURE 1 HERE

3. Methodology

Ground penetrating radar (GPR) is a high-resolution geophysical method able to provide detailed images of the shallow sub-surface. This methodology is based on the recording of EM reflections, with operative frequencies for geoscience applications generally between 10 MHz and 1000 MHz, depending on the transmitting and receiving antennae. The GPR reflections rise from dielectric permittivity contrasts between the subsurface targets and the surrounding media, which in geological and archaeological applications typically correspond to geo-lithological changes or water content variations (Jol, 2009). In low conductivity materials ("low-loss"), the maximum investigation

Deleted: Iside

Deleted: Several seismological and

Deleted: Valenzise

Deleted: Galli et al. 2006;

Deleted: 2008

Deleted: ; Brozzetti et al. 2017a

Deleted: 2002

Deleted: .

Deleted: area

Deleted: splay

Deleted: and the structures bounding the Campotenese basin have ...

Deleted: recently

Deleted: ,

Deleted: f

Deleted: pattern on

Deleted: border

Deleted: b,c

Deleted:

Deleted: east

Deleted: blue

Deleted: The Campotenese Fault (VCT) is the westernmost splay of a SW-dipping fault referred to as Rotonda - Campotenese fault, which develops in a N160E average strike-direction and includes several right-stepping en-echelon segments (Fig. 1b). The VCT extends from the southern border of the Mercure basin to the SW boundary of the Campotenese basin (average strike ~N155E) for ~15 km. Across its northern segment, an associated throw of ~120 m has been assessed based on the displaced stratigraphic boundaries mapped within the bedrock (passage between Triassic dolostones and Jurassic limestones). In this same sector, prevailing dip-slip kinematics has been documented by Brozzetti et al. (2017a).

Deleted: east

Deleted: lization

Deleted: >

Deleted: whereas is very thin (generally < 2-3 m) in the ...

Deleted: ,

Deleted: events of the

Deleted: activity

Deleted:

Deleted: mainshock

Deleted: Ultimately, based on the available surface data ...

Deleted: P

Deleted: R

Deleted: Em

Deleted: echoes

Deleted: materials (Davis and Annan 1989)

depth is generally comprised within few tens of meters (Davis and Annan, 1989). The latter is however controlled also by the electrical conductivity, which for high values causes radar signal attenuation (Annan, 2001). The reflections are recorded as a function of the Two-Way-Travel time (TWT) propagation, and displayed as a 1D GPR trace. Several GPR traces displayed along a transect build-up a radar profile or “radargram”, that is the 2D representation of the GPR reflections, more commonly identified as the conventional GPR output. A GPR dataset may be provided also as a 3D volume, which has been common for 25+ years in research applications and recently more widespread due to a wider diffusion of commercial GPR instruments equipped with arrays of antennae. The GPR is used in many research and applied fields, such as geological, sedimentological, geomorphic, hydrogeological applications (Bristow and Jol, 2003; Jol, 2009), and also in archaeological and engineering studies (Conyers, 2016; Daniels, 2004; Goodman and Piro, 2013; Utsi, 2017). In active tectonic context, several 2D/3D GPR studies have already imaged buried tectonic structures. These studies have shown geophysical images of faulting, supporting and/or extending outcrop, borehole, trench data, and contributing to base-knowledge of seismogenic structures as well as to the seismic hazard assessment of several regions around the world. Among the pioneers, we can mention Benson (1995), Smith and Jol (1995), Busby and Merriitt (1999), Cai et al. (1996) and Liner and Liner (1997), and on the successive twenty years, other 2D GPR studies were achieved across several faults worldwide (Audru et al., 2001; Demanet et al., 2001; Overgaard and Jakobsen, 2001; Bano et al., 2002; Liberty et al., 2003; Reiss et al., 2003; Slater and Niemi, 2003; Malik et al., 2007; Wallace et al., 2010; Yalciner et al., 2013; Imposa et al., 2015; Anchuela et al., 2016; Nobes et al., 2016; Matos et al., 2017; Pousse-Beltran et al., 2018; Zajc et al., 2018; Zhang et al., 2019 and Shaikh et al., 2020). In Italy, only a few GPR studies are currently available across normal faults (e.g. Salvi et al., 2003; Jewell and Bristow, 2006; Pauselli et al., 2010; Roberts et al., 2010; Ercoli et al., 2013a, 2014; Bubeck et al., 2015; Cinti et al., 2015). Over time, 2D GPR acquisitions were flanked by an increasing number of pseudo-3D or full-3D GPR studies (Grasmueck et al., 2005). Grasmueck and Green (1996) traced the future path of three-dimensional GPR applications, providing a dense 3D GPR volume to image fractures in a Swiss quarry. The study opened the possibility to three-dimensional GPR imaging of subsurface geological structures. Successive studies extended the approach to characterize active faults in different tectonic regimes combining 2D and pseudo-3D GPR surveys (e.g. Gross et al., 2002, 2003, 2004; Green et al., 2003; Troniche et al., 2006; McClymont et al., 2008, 2009, 2010; Vanneste et al., 2008; Christie et al., 2009; Carpentier et al., 2012a,b; Malik et al., 2012; Brandes et al., 2018). A review of the near-surface GPR faulting studies suggests some reflection characteristics as possible indicators for the detection of subsurface fractures and faults (e.g. Smith and Jol, 1995; Liner and Liner, 1997; Reiss et al., 2003; Gross et al., 2004; McClymont et al., 2008, 2010 and Bubeck et al., 2015). Among these, sharp lateral reflectivity variations, interruptions of the reflections, and the presence of hyperbolic diffractions are considered convincing evidence, as shown also by numerical simulations (Ercoli et al., 2013a; Bricheva et al., 2021). In addition, we have accounted for additional GPR indicators identified for Quaternary faulting in similar environments (Ercoli et al., 2013a,b; 2014; 2015), which are linked to the geometry of stratigraphic deposits across fault zones: i) reflections abrupt truncating and offsetting along sub-vertical discontinuities (especially in the case of a normal fault); ii) reflection packages thickening as they approach the fault strands; iii) abrupt lateral dip variation of the reflections; iv) peculiar reflection package geometries, with contorted reflection patterns resembling “colluvial wedges”, which McCaipin (2009) defines as deposit due to “subsidence and sedimentation of the hangingwall and erosion of the morphological scarp in the footwall”; v) localized strong GPR signal attenuation due to the presence of conductive media within the main fault zone.

Based on the research and criteria reviewed above, we carried out a near-surface interpretation of faulting based on the co-existence of most of these features along several adjacents analyzed GPR profiles. These conditions strengthen

Deleted: range

Deleted: the

Deleted: first

Deleted: or less

Deleted: .

Deleted: 2006

Deleted: , 2016

Deleted: S

Deleted: A

Deleted: surveys

Deleted: have been acquired

Deleted: Italian

Deleted: in Italy

Deleted: such

Deleted: studies

Deleted: 2000,

Deleted: Horstmeier et al., 2005;

Deleted: (likelpossibly associated with colluvial wedges).

Deleted: our fault

Deleted:

Deleted: of

Deleted: within

Deleted: the

Deleted: near-surface

Deleted: faulting

the interpretation of each profile and aids to highlight the spatial continuity of the interpreted structures over linear distances of at least many tens, or hundreds, of meters.

3.1 GPR and GNSS survey

Three different geophysical field campaigns carried-out during the 2014-2015 years, a dataset of 49 GPR profiles was acquired in the southern sector of the ROCS across the VCT fault segment (Fig. 1b-c), covering a buffer zone of ~ 400 m and ~ 200 m respectively along and across the fault strike (area of ~ 8 Ha), for a total linear length of GPR profile about 4100 m collected using a Common Offset (CO) configuration (Fig. 2).

FIGURE 2 HERE

We used a Zond 12e GPR system equipped with 300 and 500 MHz antennae. The lower frequency antennae was ultimately preferred and considered the best trade-off between maximum resolution and achievable signal penetration (in our case ~ 4 m) concerning the surveyed materials and wanted subsurface structures. The GPR was equipped with an odometer wheel to measure the radar profiles' length and with a Topcon GR-5 Global Navigation Satellite System (GNSS) receiver to achieve accurate positioning of GPR traces and profile. Considering the scarce presence of obstacles across the survey site and the good satellite coverage, we opted for a Network Real-Time Kinematic positioning (NRTK, connected to the NETGEO network), measuring coordinates and elevations with centimetre accuracy, and stored directly within the SEG-Y GPR files.

Three datasets were acquired after preliminary fieldwork and collection of geological structural data at the surface and which allowed us to infer the possible location of the fault trace. The average NE-SW direction of the GPR lines was initially planned with the primary purpose of intersecting the VCT fault ~perpendicularly to its SW-NE strike, as reported by literature and visible by surface evidence. This solution theoretically allows a more reliable interpretation of the investigated structure by reducing the effect of the apparent dip-direction and dip-angle of both stratifications and faults.

The acquisitions carried out in 2014, first resulted in twelve SW-NE GPR profiles collected in the southern sector of the basin (CMT light-blue lines in Fig. 2a), which was a flat land characterized by Quaternary alluvium. The second acquisition encompassed four additional radar profiles collected in the same area, and another nine radar profiles progressively moving to north, which were collected with slightly different and converging orientations in the central sector (CMT green lines Fig. 2a). This solution was pursued for two main reasons: 1) to avoid directly surveying the outcropping dolostones (only partially crossed with two northernmost profiles) characterizing two hills $h1$ and $h2$ (dashed white polygons in Fig. 2), and thus focussing only on the sedimentary cover which is our target for possible Quaternary faulting; 2) to optimize, through a preliminary GPR data interpretation, the future acquisition schemes by figuring out the dip direction of the buried geologic structures of interest. In fact, similarly to the interpretation of reflection seismic profiles, the "apparent dip" of reflections in bidimensional radar profiles should be considered to achieve a reliable 3D conceptual model.

In order to intercept several possible buried faults and fault-related structures as well as to fully image the local structural setting, the successive 2015 acquisition crossed part of the Triassic dolostones ridge with longer GPR profiles. The GPR profiles collected during the second 2014 campaign (close to $h1$ and $h2$) already revealed a considerable difference in GPR reflectivity between the unconsolidated deposits and layered and fractured Mesozoic lithotypes (Gafarov et al., 2018). Therefore, two new datasets of 24 parallel GPR radar profiles (CMT dark-blue sets

Deleted: ¶

Deleted: The GPR profiles were acquired across the VCT fault (Fig. 1c), during three different geophysical campaigns in the years 2014-2015 (Fig. 2). The entire dataset encompasses 49 radar profiles (linear length of about 4100 m) collected with a Common Offset (CO) configuration.

Deleted: The first

Deleted: About t

Deleted: the

Deleted: , using subsurface

Deleted:

Deleted: r

Deleted: effective "apparent

Deleted: "

Deleted: the

Deleted: all

Deleted: buried

Deleted: an ideal along-dip acquisition cannot be always achieved and ...

Deleted: is

Deleted: , to

Deleted: also in the interpretation of 2D GPR images aiming to obtain a 3D (similar to the interpretation of reflection seismic profiles).conceptual model.

Deleted: Preliminary results shown by

Deleted: parallel

1 of lines in Fig. 2a, north “n” and south “s”) were extended in NNE-SSW and NE-SW directions, respectively,
2 crossing *h1* for several tens of meters (max profile length ~220 m) throughout the basin. The GPR profiles were
3 recorded using a trace step of 0.05 m and a profile inter-distance of 25 m for dataset “n” and 10 m for dataset “s”,
4 respectively. A detailed summary of the acquisition parameters used for the GPR surveys is reported in Table I. For
5 these two datasets, the profile spacing and positioning are more regular and accurate, thanks to a preparatory transects
6 planning using a GIS project. Thus, we later staked out their initial and final positions during the fieldwork through
7 the differential Global Navigation Satellite System (GNSS). The results of the accurate GPR traces positioning
8 achieved during the GNSS campaigns were also later used for GPR data processing, visualization, and interpretation.

9 TABLE 1 HERE

10 **3.2 GPR data processing and results:**

11 The processing sequence was customized after testing several workflows and parameters. We aimed to remove random
12 and coherent (e.g. ringing) noise and enhance the data quality to better visualize the geometry of the buried reflections
13 and their discontinuity in signal amplitude and phase. The first step was an accurate Quality Control (QC) of the
14 profile coordinates and topographic profiles. Although the generally favorable environmental conditions (e.g. good
15 satellite coverage, no forested areas etc..) of the site for a GNSS survey, some measurements were occasionally
16 suffered a degradation of positional accuracy (e.g. temporary scarce satellite coverage or poor communication via
17 Network Transport of RTCM via Internet Protocol - Ntrip). For some traces therefore the coordinates and elevation
18 field records that were outliers (Fig. 3a) were corrected using various strategies (e.g. replacement, interpolation, or
19 smoothing, Fig. 3b).

20 FIGURE 3 HERE

21 We have also compared our measurements with topographic transects extracted from a 10 m and a 5 m resolution
22 Digital Terrain Models (DTM) by Tarquini et al. (2012) and by Regione Calabria. Later on, we finally used a 1 m
23 resolution DTM (Geoportale Nazionale, Lidar data provided by Italian Ministero dell'Ambiente e della Tutela del
24 Territorio e del Mare - MATTM) to double-check if, despite the different scales of observation, the topographic
25 profiles were comparable. Although the metre resolution of the DTM is unable to represent centimetre topographic
26 variations, the comparison confirmed an excellent match of the topographic profiles at a meter scale, so that the DTM
27 data were integrated to correct the GNSS measured topography when the accuracy of GNSS recordings were
28 excessively degraded. With the topographic profiles corrected, the raw GPR data (Fig. 3c, illustrating the profile
29 cmt5s) were initially processed with the Prism software (Radar System, Inc., <http://www.radsys.lv/en/index/>) using a
30 basic processing sequence, to analyze the main characteristics of data and optimize a customized processing flow. The
31 processing sequence was later improved through ReflexW software (<https://www.sandmeier-geo.de/reflexw.html>, see
32 Table II for details on the processing algorithms and parameters). The workflow included a time-zero correction,
33 dewow, amplitude recovery, velocity analysis, background removal, bandpass filtering, F-K filtering, 2D time
34 migration, topographic correction, and time-to-depth conversion. The amplitude recovery was operated through a
35 “gain function” including a linear and an exponential coefficient ($g(t) = (1+a*t)*e^{(b*t)}$) to enhance the amplitude
36 (reflectivity) contrasts as well as preserving the horizontal and vertical amplitude variations already visible in the raw
37 data (Fig. 3a). This amplitude recovery function was used across all the profiles with slight customization depending

Deleted: distance
Deleted: 10
Deleted: 25
Deleted: in the field during
Deleted: new grids
Deleted: Geographic Information System Information System (...
Deleted:)
Deleted:
Deleted: also

Deleted: s
Deleted: a,

Deleted: by

on the datasets (details in table II). The entire processing flow was applied to all the available radar profiles, again with occasional filtering adaptations aiming to remove local pervasive signal ringing (e.g. due to low antennae-ground coupling). Particular care was dedicated to the migration process, whose algorithm was decided after extensive tests on several radar profiles to select the best migration strategy.

TABLE 2 HERE

In fact, a very different reflectivity and maximum depth of penetration are visible in the data: it is more than 150 ns in the central sector, reducing to 70-80 ns in the rest of the radar profiles (Fig. 3c): this fact suggests sharp lateral variations of subsurface media (Figs. 3d) and possibly of the velocity field. Thus, we have first tested a 1D time migration algorithm (Kirchhoff) performing a Migration Velocity Scan (MVS) analysis (Forte and Pipan 2017) and inspecting the success of diffraction hyperbola collapse after migration. We have varied constant values of EM velocity, from a minimum of 0.06 up to 0.12 m/ns, with steps of 0.01 m/ns, to evaluate considerable variation in dielectric properties of surveyed media. The MVS is characterized by a higher velocity for the central sector of the GPR profiles which displays high reflectivity: Fig. 4 illustrates an example of the migration results obtained on the profile cmtIn_a, by using three constant values of average velocity. The profile in Fig. 4a shows the unmigrated version characterized by numerous hyperbolic and half hyperbolic diffractions originated by single scatter points and wavy reflections (white arrows). In Fig. 4b we display the first test using $v = 0.07$ m/ns, showing overall good results, with slightly under-migration at a few points mainly located within the shallower sediments (light-blue arrows). The hyperbolic diffractions are also nicely collapsed using higher velocity ($v = 0.09$ m/ns) as shown in Fig. 4c (dark-blue arrows), even if some imaging problems affect deeper reflections. The last migration scan test ($v = 0.11$ m/ns) displays a good result only in few profile sectors (dark-blue arrows), particularly localized within the sectors with high reflectivity, displaying an improved lateral reflection continuity. The rest of the radar profiles show generally poor imaging, particularly in the area characterized by strong attenuation, where the wavy reflection is over-migrated (red arrows indicating migration smiles, Fig. 4d).

FIGURE 4 HERE

The workflow, therefore, suggests a challenging imaging task, due to velocity variation happening not only in depth as well as laterally across the different media. This sharp change of reflectivity and velocity at a distance of about 13-14 m (Fig. 4d) represents a complex problem for the efficiency of 1D migration algorithms standardly used for GPR imaging. Such considerations has lead testing a 2D migration algorithm, by creating and using a 2D velocity model obtained for each radar profile through a hyperbolic diffraction fitting tool (Fig. 5a). Single velocity points have been fitted for each area, displaying hyperbolic diffractions, while in the remaining parts of the radar profiles we have arbitrarily included presumed velocity adaptation only to obtain a regular grid of points to spatially interpolate the 2D models. The 2D migrated radar profiles, in comparison to the 1D approach, resulted in improved imaging of GPR profiles, displaying a more accurate collapse of the hyperbolic diffractions into point sources and an improved relocation of dipping reflections, with a refinement of their geometry and an increase of their continuity. A good-quality imaging result is visible on the central sectors of radar profiles displaying strong reflectivity and reflections with improved continuity, but also many phase breaks and displacements. Despite steep topographic gradients, sharp lateral velocity variation and the reflection heterogeneity might cause imaging issues that need to be treated using more specific workflows (Lehmann and Green, 2000; Heincke et al., 2006; Goodman et al., 2007; Dujardin and Bano,

Deleted: Em

Deleted: highlighted

Deleted: extract

Deleted: are rising on

Deleted: s

Deleted: clearly

Deleted: ,

Deleted: ,

Deleted: have

Deleted: driven

Deleted: to

Deleted: clearly

2013). We believe we have reached a good compromise for our purposes. In our case, a considerable improvement, can be seen along the hill-slope and flatter areas (profile cmt1n_a, Fig. 5b) which are of greatest interest for the study aimed at detecting possible earthquake ruptures within the Quaternary deposits. The improved imaging of reflection geometries is therefore fundamental for the interpretation and detection of geophysical signatures of faults.

FIGURE 5 HERE

A successive import of the processed SEG-Y data was done into the seismic interpretation software OpendText Pro v.6.4 (Academic license courtesy of dGB Earth Science, <https://www.dgbes.com>), which was used first for global quality control of processing operations (correctness of topographic correction and datum plane, coordinates accuracy and matching, profiles orientation and intersection) and for three-dimensional (3D) visualization of all the profiles (Fig. 6a). The three-dimensional GPR project was subsequently integrated with geological and structural maps, DTM, and literature schemes (using a common Coordinate Reference System: WGS84 UTM Zone 33N, EPSG: 32633) in the Move suite software v. 2019.1 (Academic license courtesy of Petroleum Experts, <https://www.petex.com/>) for GPR interpretation and model building. All the E and W-dipping fault surfaces were created interpolating the fault-sticks picked on displaced reflections and correlated across adjacent radar profiles. In particular, we used the "surface geometry" tool to extract the properties of each single mesh building up the surfaces, and obtaining the "dip" and "dip azimuth" data. Subsequently, such values have been automatically saved in an attribute table, which can then be queried to reconstruct the "synthetic" stereonet.

4. GPR data description and interpretation

The 3D MOVE project allowed us to extract 2D and 3D data visualizations to better figure out the relationships between the main reflections identified on the different GPR profiles (Fig. 6a). The workflow aimed to reconstruct and model the three-dimensional surfaces including both horizons and high-angle discontinuities.

FIGURE 6 HERE

A common feature on all the radar profiles is the strong reflectivity visible within their central sectors (e.g., profile cmt3n in Fig. 6b), which are characterized by an irregular and steep slope, particularly within the northern portion of the surveyed area. These sectors show deep GPR signal penetration due to the Triassic dolostones, which outcrop in the central and northern portions of the study area (Figs. 1c and 2a). The quality of the radar reflections and the remarkable depth reached (~ 6 m, Fig. 6b) suggest this rock type is an excellent dielectric medium (corresponding to higher frequency content zone in the 2D spectrum of Fig. 6c). However, its reflection pattern is not spatially homogenous, being characterized by oblique and sub-parallel reflections. The latter are interpretable as dolostone beds of moderate (25-30°) W and E "apparent" dip on the respective sides of the surveyed dolostone hills. In addition, these reflections are frequently cut and slightly displaced by apparent high-angle (60-65°) phase discontinuities, highlighted by a dense hyperbolic diffractions pattern (radar profile cmt2n, Fig. 7a) suggesting intense fracturing and little faults displacing the dolostone (Fig. 7b). This radar signature was recorded not only in correspondence of the outcropping carbonate but also in the transition slope areas covered just by a thin soil layer (Figs. 7b,c). In the southern side of h1, an outcrop with thin microbialitic laminae allows one to measure the attitude of the bedding (NNW dip, ~ 30-35° dip

Deleted: , w

Deleted: ¶

Deleted: the

Deleted: east

Deleted: west

Deleted: ¶

Deleted: of the radar profiles acquired across the VCT fault trace and allows us

Deleted: data

Deleted: ,

Deleted: more

Deleted: er

Deleted: characterized bywith

Deleted: areas

Deleted: are

Deleted: caus

Deleted: ed

Deleted: by

Deleted: In the southern side of h1, thin microbialitic laminae allows one to measure the attitude of the bedding, which shows a NNW dip (~ 30-35°). In the same area, we measured two sets of major and minor joints, both with a dip angle of ~ 40-45° degrees and a SW and SE dip, respectively.

Deleted: Looking at t

Deleted: at

Deleted: (~ 6 m, Fig. 6b)

Deleted: by the GPR signal

Deleted: ,

Deleted: that

Deleted: represents

Deleted: often

Deleted: s

Deleted: ,

Deleted: displaying

Deleted: west

Deleted: east

Deleted: also

Deleted: .

Deleted: We, interpreted these features as sets of joints or minor faults

Deleted: ing

Deleted: layers

angle) as well as two sets of major and minor joints (SW and SE dip and dip angle of ~ 40-45°, respectively) fitting with GPR reflections.

Apart from its internal heterogeneities, the GPR signature of the Triassic dolostones can be considered as a well-defined depositional facies (*fc1*) (Sangree and Widmier, 1979; Huggenberger, 1993; Beres et al., 1999; Jol and Bristow, 2003). A different radar signature *fc2* is defined for the profile sectors on the sides of *fc1*. This second facies is characterized by prominent laterally-continuous and sub-parallel reflections in the very shallow depth range (< 1 m, just beneath the direct arrivals), stratigraphically sealing underlying reflections 1-3 m deep: the latter are more discontinuous, wavy, and contorted, with moderate to low reflectivity and encompassing sparse diffraction hyperbolas (in unmigrated data, Fig. 7a). This reflection pattern overlaps onto a generally prominent wavy reflection (Figs. 7a,b), which typically marks the transition to strong signal attenuation deeper in the section.

FIGURE 7 HERE

The reflection package belonging to *fc2* corresponds to the alluvial/colluvial deposits (Fig. 7b,d), outcropping on the sectors with flat topography, which represent the GPR profile sectors we've carefully inspected to find for geophysical evidence of Quaternary faulting. A key-layer for this research is the described prominent wavy reflection, as it can be recognized in many radar profiles. The related interpretation is not straightforward in the absence of direct data (e.g. boreholes and/or paleoseismological trenches) or at least without additional geophysical data. A strong GPR reflection suggests significant variation of the dielectric constant between the two media so that most of the incident energy is reflected back to the receiver at the surface. This wave behaviour is potentially explained by several geological models, such as: i) a high dielectric contrast may be a result of a sharp soil moisture variation (Ercoli et al., 2018); ii) a sharp erosional, stratigraphic or tectonic boundary within heterogeneous deposits (Ercoli et al., 2015), or iii) a contact between two considerably different lithologies, such as unconsolidated deposits laying above a bedrock substrate reflecting back all (or almost all) the incident signal (e.g., Frigeri and Ercoli, 2020). In addition, the possible role of conductive deposits (e.g. high clay content) should not be discounted to explain the occurrence of strong attenuation. Several considerations are at the basis of the GPR data interpretation.

1) the available well logs show the Pleistocene-Holocene alluvium and colluvium layered above the carbonate bedrock ~20-30 m depth (Brozzetti et al., 2017a), a greater depth than the strong GPR reflection. However, it should be observed that the area drilled is located ~2.5 km away on the north-westernmost sector, over the depocenter of the Campotenesse basin, whereas the studied GPR site is placed just on its eastern border, in proximity to emerged dolostone hills; 2) only terraced Middle-Pleistocene silts and sands (Schiattarella et al., 1994) and slight coatings of Late Pleistocene colluvium (generally < 2 m thick) are documented to outcrop in the eastern sector of the basin (footwall of VCT fault) (see Fig. 7 in Brozzetti et al., 2017a); 3) the subsurface geometries highlighted by the prominent GPR reflection and underlying reflection pattern suggest a relatively thin layer of sedimentary deposits resting on a fractured substratum. Its top surface is progressively deepening towards the W, thus providing increased space for settling sediments, and thus a gradual thickening of deposits is observed from E to W.

In light of the above considerations, we interpret the prominent wavy GPR reflection as a buried top layer of carbonate (e.g. as observed e.g. by Bubeck et al., 2015), in our case represented by the Triassic dolostone formation. The latter is lying at a shallower depth (1-3 m) beneath shallow and poorly consolidated Quaternary deposits, across both sides of the surveyed hills. Thus, after picking such a prominent reflection event on all the radar profiles, the top of bedrock surface was reconstructed as shown in Fig. 8a (coloured surface). In this figure, we display also an overlay of a recent

- Deleted: This radar signature was recorded not only in ...
- Deleted: This radar signature was recorded not only in ...
- Deleted: on the sides of *fc1*
- Deleted: GPR facies (*fc2*) is
- Deleted: prominent
- Deleted: ...just beneath the direct arrivals (< 1 m ...
- Deleted: which ...stratigraphically seals ...
- Deleted:
- Deleted: in a depth-range the ...-3 m deep: the latter ...
- Deleted: reflections... of ...
- Deleted: with ...ncompassing numerous ...
- Deleted: are visible in the 1-3 m depth-range (variable ...
- Deleted: and
- Deleted: . Below this reflection pattern ...which typically ...
- Deleted: more in depth
- Deleted: ¶
- Deleted: We have classified the
- Deleted: overall radar signature of
- Deleted: these ...eflection package...package belonging to ...
- Deleted: several
- Deleted: clearly ...ot straightforward in the absence of dir ...
- Deleted: . The related interpretation is not straightforward ...
- Deleted:A strong GPR reflection suggests significant ...
- Deleted: (e.g., Frigeri and Ercoli 2020)
- Deleted: sediments within layered ...eposits (e.g. high cla ...
- Deleted: signal attenuation
- Deleted: ¶
- Deleted: To support ...he GPR data interpretation:, some ...
- Deleted: : 1) stratigraphy of two water wells located only ...
- Deleted: T
- Deleted: area
- Deleted:
- Deleted: of the
- Deleted: basin
- Deleted: calcareous ...olostone hills;. ...
- Deleted: In addition,
- Deleted: it should be mentioned that
- Deleted:
- Deleted: of ...f VCT fault) (see Fig. 7 in Brozzetti et al., ...
- Deleted: ¶
- Deleted: , whose ...op surface surface ...
- Deleted: west
- Deleted: . For this reason, a...and thus a gradual deposits ...
- Deleted: east ... to west
- Deleted: Therefore...n light of the above considerations, v ...

1 structural map of the basin (modified after Brozzetti et al., 2017a) reporting the area dissected by a set of en-echelon
 2 fault splays to the West associated to the VTC segment. Thus, analyzing the geophysical characteristics of the
 3 prominent, wavy reflection in terms of a structural interpretation, the main peculiar characteristic is the clear “stepped”
 4 geometry of some sectors (Figs. 5b, 6b, 7b, 8b), namely breaks of its continuity associated to lateral sharp variations
 5 of depth (linked to sediment growth and onlaps). We also notice other geophysical features, which can be observed in
 6 the stratigraphy of overlying deposits (fc2): some reflections are semi-continuous to discontinuous (sharp variation in
 7 signal amplitude and phase), and display evident lateral variation of the dip angle.

8 FIGURE 8 HERE

9 These broken reflection packages present truncations (e.g. Smith and Jol, 1995), displacements, and hyperbolic
 10 diffraction events (insets of Fig. 8b1,b2). Such peculiar GPR signature is therefore compatible with coseismic
 11 displacement due to Late Quaternary surface faulting events (Fig. 8b). Contorted reflections across the main
 12 discontinuities frequently show localized strong attenuation of GPR signal (Fig. 8b). The attenuation might be linked
 13 to their high dip-angle, causing a minor amount of energy being reflected back to the antenna, but, more likely, due to
 14 the presence of conductive fine soils nearby faulted zones (e.g. circle 1 in Fig. 8b). These conditions can be linked to
 15 different depositional facies across fault zones (McClymont et al., 2010) e.g. including colluvial wedges (Reiss et al.,
 16 2013; Bubeck et al., 2015) or deposits deriving from degradation of fault scarps (detailed interpretation within the
 17 caption of Fig. 8b). Using all such stratigraphic evidence and geophysical markers of faulting, we have therefore
 18 interpreted and classified synthetic (W-dipping, blue) and antithetic (E-dipping, red) normal faulting events (Fig. 8b).
 19 During the interpretation process, the faults were picked using solid lines (fault sticks); when the presence of
 20 geophysical markers of faulting were uncertain, a dashed fault segment was initially added and revised a second time
 21 their possible connection among nearby GPR profiles.
 22 The interpreted faults present a dip angle between 65-75° and variable amount of displacement (D), estimated by
 23 correlating the position of the top of the carbonate substratum in the footwall and hanging wall blocks (e.g. scheme
 24 summarized in the inset of Fig. 8b3). Considering the GPR profile of Fig. 8 as representative for the studied VCT
 25 sector, D is not exceeding ~1 m for the W-dipping splays within the Quaternary sediments (~0.5 m for the E-dipping
 26 splay). A displacement D of ~1.5 m was derived across the sharp boundary between the Triassic dolostone and the
 27 Quaternary deposits (easternmost fault on Fig. 8b), being interpreted as the main fault. This clear contact is
 28 characterized in all profiles by hyperbolic diffractions (in unmigrated data), variable dip angle, abrupt truncations,
 29 sharp lateral variation of the reflectivity suggesting a wide fault zone (Figs. 3 to 9), controlling the above mentioned
 30 Quaternary splays. By interpolating all the fault sticks placed in adjacent profiles, we have created the fault surfaces,
 31 that show a good degree of continuity, from north to south (Fig. 9). For the studied sector of the VCT, we have
 32 reconstructed the tridimensional fault-network and the geometry of the associated synsedimentary deposits at a metric
 33 scale of observation (Fig. 9).

- Deleted:** ¶
- Deleted:** shows
- Deleted:** are...the...sectors with a ...lear “stepped” geometry of some sectors (Figs. 5b-... 6b-... 7b-... 8b), namely sharp ...reaks of its continuity associated to lateral sharp depth
- Deleted:** highlighting abrupt lateral variations in depth and in its thickness
- Deleted:** fc1...c2): some reflections are semi-continuous to discontinuous (sharp variation in signal amplitude and phase)...and displaying...evident lateral dip
- Deleted:** In some sectors t...hese broken reflection packages present truncations (e.g. Smith and Jol, 1995), v...isplacemenetical offse
- Moved (insertion) [2]**
- Deleted:** possible ...o-...eismic displacement due to Late Quaternary surface faulting events (Fig. 8b). Contorted reflections across the main discontinuities frequently show localized strong attenuation of GPR signal (interpretation summarized in caption of ...ig. 8b), which... The attenuation might be linked to their high dip-angle, causing a minor amount of energy being reflected back to the antenna, but, more likely, due to the presence of conductive fine soils across ...earby faulted zones (e.g. circles...1 and 2 ...n Fig. 8b). These conditions can be linked to different depositional facies across fault zones (McClymont et al., 2010) e.g. including colluvial wedges wedges ...Reiss et al., 2013; Bubeck et al., 2015) or deposits deriving from degradation of fault scarps (detailed interpretation within the caption of Fig. 8b))
- Moved up [2]:** Such peculiar GPR signature is therefore compatible with possible co-seismic displacement due to Late Quaternary surface faulting events (Fig. 8b).
- Deleted:** west...-dipping, blue) and antithetic (east
- Deleted:** within the Quaternary sediments ...Fig. 8b). During the interpretation process, t...e interpreted
- Deleted:** a vertical offset... is ranging from a few tens of centimeters up to...ot exceeding ~1 ...eter...for the W-dipping splays within the Quaternary sediments (~0.5 m for the E-dipping splay), and were picked using solid lines (fault sticks... A displacement D of ~1.5 m was derived). During the interpretation process, when the presence of geophysical markers of faulting were uncertain, a dashed fault segment has beenwas initially added and only later analyzed a second time by looking at their possible connection with nearby lines. ...In addition to the fault sticks within the Quaternary sectors, we placed main fault sticks ...cross the sharp boundary between the Triassic dolostone and the Quaternary sediments...eposits (easternmost fault on Fig. 8b), being interpreted as the main fault)...These...clear contact is generally ...haracterized in all profiles by by fractured zones including ...yperbolic diffractions (in unmigrated data), contorted reflections geometry of ...ariable dip angle, abru...
- Deleted:** ,...from north to south (Fig. 9). ¶
Our geophysical interpretation allowed
- Deleted:** , thus ... reconstructing ...f...r this
- Deleted:** ,
- Deleted:**
- Deleted:** a higher resolution

5. Discussion

5.1 Inferences from subsurface 3D model

The perspective view of Fig. 9a shows a 3D structural scheme of the main tectonic lineaments at the basin scale displaying a NW-SE faults strike (modified after Brozzetti et al., 2017a) in relation to the GPR investigated area (white rectangle). Our GPR interpretation enriches many of the details such a former structural scheme across the southern VCT segment. We highlight an en-echelon system of two main SW and NE-dipping faults, as well an articulated set of extensional meso-faults within the Quaternary sediments. The high-angle GPR discontinuities identified in the study (e.g., Fig. 9b), show a considerable continuity in the NW-SE direction (accurate 3D structural reconstruction in Fig. 9c), dissecting not only Quaternary alluvial-colluvial deposits (except for the very shallow $fc2$ layers), but also deeper stratigraphic layers.

The reconstructed faults mark a horst-graben structure, mostly buried within the Campotenesse basin, which locally emerges from the Quaternary deposits. In the investigated area it corresponds to a NNW-SSE elongated topographic high ($h1$ and $h2$ in Fig. 2a) made by the Triassic dolostone. This horst is bordered toward the W and towards the E by SW- and NE- dipping normal faults, respectively (Figs. 9b, c). In Fig. 9c, the fault-set $d1$, together with its antithetic set $d2$, shows the maximum displacement and the most evident deformation of the adjacent sub-surface deposits. The variations of thickness of such Quaternary deposits are consistent with the horst and graben configuration. Thinning is observed in correspondence with the raised buried blocks, whereas thickening, wedge-shaped as well as chaotic geometries correspond to the lowered blocks. The main fault of set $d1$ can be considered a conjugate fault of the VCT (Fig. 8b), separated by a right step-over of about 0.5 km from the segment that borders the eastern basin (Figs. 2c, 8a). Thus, also the fault-set $d3$ and $d4$ located on the eastern part of $h1$ and $h2$, can be hierarchically classified as a network of minor splays embedded in the southern junction zone between the two VCT segments (Fig. 9c). The three-dimensional model (Fig. 9a,c) highlights that these faults, despite having a typical Apenninic NW-SE trend, are characterized by a complex polymodal pattern of strikes, with alternating N-S to NW-SE direction. Therefore, such a polymodal character, which was observed along all the extensional structures of the area (Brozzetti et al., 2017a) is also confirmed at the GPR scale along this VCT sector. A dedicated statistical analysis of the reconstructed fault planes is reported in the stereo plots of Fig. 9d ($d1$ - $d3$ = W-dipping faults; $d2$ - $d4$ = E-dipping faults).

FIGURE 9 HERE

5.2 Seismic hazard implications

The combination of geological and seismological data may suggest outcropping Quaternary faults being capable of releasing earthquakes, but the determination of the maximum expected magnitude along these faults might not always be well constrained. An estimate can be made using well-known scale-relationships (Wells and Coppersmith, 1994; Wesnousky et al., 2008; Leonard, 2010; Stirling et al., 2013) with knowledge of the geometric parameters (e.g. fault length, area and depth), which are often difficult to assess. These scale relations can also be applied also to Quaternary scarps originated by cumulative coseismic faulting produced by medium-strong earthquakes (generally $M > 6$). Nevertheless, only through paleoseismological analysis is it possible to distinguishing the amount of slip due to each event. But in cases like the VCT, GPR provided key parameters where no direct information on the nature of the surveyed deposits and no accurate dating is available, at the present day, the GPR data assume a key-value. Our GPR

Deleted: The 3D map views of Fig. 9 show a structural scheme of the main fault lineaments in the basin displaying a NW-SE strike. Our interpretation highlights an en-echelon system of main SW and NE dipping faults on both sides of the hills where the Triassic dolostones crop out, as well as several secondary structures within the Quaternary sediments.

Deleted: performed ...riches of ...any of the details such as such a ...former structural scheme across the studied ...outhern VCT segment. We highlights ...an en-echelon system of two main SW and NE-dipping faults on both sides of the Triassic dolostones hills, ...as well as ... articulated set of extensional meso-faults several secondary structures ...ithin the Quaternary sediments. The high-angle GPR discontinuities identified in the study (e.g., Fig. 9b),

Deleted: ing

Deleted: at shallow depth

Deleted: deeper reflections referred to

Deleted: , show a considerable continuity in the NW-SE direction (Fig. 9c). These structures can be interpreted as the sub-surface expression of an articulated set of extensional meso faults associated with the VCT

Deleted: s are arranged in ...ark a horst-graben structure, mostly buried within the Campotenesse basin, which locally emerges from the Quaternary deposits. In which the higher displacements are associated to the westW-dipping faults (Fig. 9a). ... the investigated area it corresponds to a NNW-SSE elongated topographic high ($h1$ and $h2$ in Fig. 2a) made by the Triassic dolostone. This horst is bordered toward the W and towards the E by SW- and NE- dipping normal faults, respectively (Figs. 9b, c). Among these faults, the master structure in the southern sector of the basin (Fig. 9a) bound toward west a structural high where the Triassic dolostones crop out. The structural high, which corresponds to a NNW-SSE elongated topographic high ($h1$ and $h2$) elongated in the NNW-SSE direction, is also bordered towards the east E by a minor eastE-dipping normal fault (Fig. 9b). Thus, it appears as an uplifted horst showing an axis of elongation sub-parallel to the average strike of the Campotenesse basin. The horst is mostly buried within the basin but locally emerges from the Quaternary sediments, as in the central portion of the investigated area ($h1$ and $h2$ in Fig. 2a). ... In Fig. 9c, the fault-set $d1$, together with its antithetic set $d2$, ...in Fig. 9c ...hows the maximum displacements ...and the most evident deformations ...of the adjacent sub-surface deposits. The variations of thickness of such Quaternary

Deleted: n...average ...W-SE direction...rend, are characterized by a complex polymodal pattern of strikes, with alternating N-S sections...alternating ...o NW-SE sections...irection. Therefore, such a The ...olymodal character, which... is...hich was ...bserved at various both thus along the entire VCT and , ...long all all ...he

Deleted: The variations of thickness of the Quaternary deposits, detectable interpreted on the radar profiles, are consistent with the horst and graben configuration. Thinning is observed in correspondence with the raised buried blocks whereas thickening and wedge-shaped and locally chaotic geometries

Deleted: In many cases, ...he combination of geological and seismological data show ...ay suggest that...the ...utcropping Quaternary faults are ...eing capable of releasing earthquakes, but the determination of the maximum expected magnitude along these faults might notis not...always be well constrained. An estimate of ...an be made using well-know

interpretation by itself doesn't currently allow one to extract any date for a single event, neither identify a succession of past events as well as establish recurrence times (Galli, 2020). However, it confirms the segmentation of the VCT and the presence of buried splays, which appear to have exerted a strong control on the deposition of Late Quaternary sediments. The location of Quaternary ruptures at a shallow depth in a flat land of an intra-mountain basin, presently undergoing alluvial and colluvial sedimentation, suggests their occurrence might be attributed to the Holocene. Thus, pointing out normal faulting of Holocene deposits would be, in itself, a very important and novel result for the Campotenes area. A Middle-Late Pleistocene age of activity was suggested for the Mercure and Campotenes boundary faults by Schiattarella et al. (1994) and Brozzetti et al. (2017a), with Holocene activity indirectly inferred on the base of morpho-structural observations. More recently, an earthquake-structure association with the recent 2010-2014 Pollino seismic sequence has been reconstructed through cross-sections and relocated seismicity in Cirillo et al., (2021).

Our data are promising because the GPR facies interpretation highlights the possible presence of small-scale grabens or half-graben (maximum estimated fault zone width of ~ 160-170 m, inset c1 of Fig.9c) and the likely fault-related deposits (e.g. as observed by Reiss et al., 2013 and Bubeck et al., 2015), at shallow depth. This inference would testify to not only the persistence of extensional deformations up to the Late Quaternary but would even imply the occurrence of episodes of surface faulting. In other words, the Campotenes basin may have been affected in the relatively recent past by medium-strong earthquakes, larger than the 2010-2014 mainshocks. It should be in fact considered that historical events with $6 < M_w < 7$ surrounded the area, being documented a further ~ 50 km north (1857 - M_w 7.1) and ~ 60 km south (1184 - M_w 6.7, Fig. 1a) (Rovida et al., 2020). Some paleoseismological earthquakes with inferred magnitude $6.5 < M_w < 7$ are attributed to the Castrovallari fault, located ~ 20 km SE and also falling within the Pollino seismic gap (Cinti et al., 1997; Michetti et al., 1997; Cinti et al., 2002, 2015).

The estimates of the VCT fault-length provide an overall value of 15 km (Brozzetti et al., 2017a) which is compatible, in the case of a complete rupture, with the maximum expected magnitudes of $M_w = 6.45$ (Wells and Coppersmith, 1994) and $M_w = 6.8$ (Wesnousky et al., 2008 and Leonard, 2010), therefore well capable to produce surface breaks. Being the source of the most recent earthquakes (2012 - M_w 5.2; 1894 - M_w 5.1; 1708 - M_w 5.8 and perhaps 1693 - M_w 5.2) affecting the study area estimated at ~ 8 km depth (Totaro et al., 2015; Brozzetti et al., 2017a; Napolitano et al., 2020 and 2021, Sketsiou et al., 2021), the level of seismic energy released by such historical seismic events would likely be not enough to generate the VCT ruptures at surface. Therefore, it sounds reasonable that the hypothesis of past earthquakes occurrence, nucleated from the VCT, with a magnitude sufficiently high to cause the buried coseismic ruptures, highlighted by our GPR interpretation, which were then subsequently erased at surface by footwall erosion and sedimentation at the hanging wall. In addition, because historical catalogs do not show events with $M_w > 6$ (Rovida et al., 2020), a very energetic earthquake could have likely occurred before the period covered by the available seismological catalogs, proving new perspectives on the actual seismic hazard of the area.

6. Conclusions

Our novel GPR data and dedicated workflow allowed us to obtain a detailed 3D model of the southern sector of the Fosso della Valle - Campotenes fault (VCT) in the continental Campotenes basin, a seismic gap in the Mt. Pollino region (Southern Italy). The processing, analysis, assemblage, and interpretation of the 49 GPR profiles was pursued using expertise, techniques, and tools borrowed from seismic reflection industry applications. The non-destructive GPR survey did not require special authorizations and was relatively fast and low cost. The pseudo-3D configuration

Deleted: data ... confirms the segmentation of the VCT and point out ... the presence of a ... buried splays, which appears ... to have exerted a strong control on the deposition of Late Quaternary sediments, just below the present topographic surface... Moreover, we have highlighted that sediments, in turn, are affected by faulting. ... their ... location of Quaternary ruptures at ... very ... a low ... shallow depth (1 - 4 m) ... a flat land of an intra-mountain basin which is ... presently undergoing alluvial and colluvial sedimentation, suggests their occurrence might be attribution

Deleted: , as no previous study has provided this kind of evidence yet... In fact

Deleted: A ... Middle-Late Pleistocene age of activity was suggested for the Mercure and Campotenes boundary faults by Schiattarella et al. (1994) and ... Brozzetti et al. (2017a), based on morpho-structural observations... with.

Deleted: whereas

Deleted: Their ... olocene activity has been only ... indirectly inferred on the of, they assumed ... on the base of morpho-structural observations. More recently, aa according to the possible ... earthquake-structure associations ... of the faults with the recent 2010-2014 Pollino seismic sequence has be

Deleted: seem even ... re more ... romising because the GP

Deleted: ... at shallow depth (just below the present

Deleted: nucleated from the VCT, capable of producing

Deleted: are

Deleted: little

Deleted: (~50 km) ... orth (1857 - M_w 7.1) and ~ 60 km

Deleted: Guidoboni et al. 2018

Deleted: ¶

Deleted: up to

Deleted: $M_w = 7.6.5$... re attributed to the Castrovallari fa

Deleted: ; and Ercoli et al. 2015

Deleted: (Brozzetti et al. 2017a)

Deleted: capable to produce surface breaks. From using

Deleted: The result suggests that the ... e ... source of the

Deleted: which ... ffectcd

Deleted: (2012 - M_w 5.2; 1894 - M_w 5.1; 1708 - M_w 5.8 ar

Deleted: was

Deleted: a source

Deleted: . WThus, ith this hypocentral depth

Deleted: the ... he level of seismic energy released by such

Deleted: ¶

Deleted: B... cause historical catalogs do not show events

Deleted: probably ... very energetic earthquake could hav

Deleted: ¶

Deleted: ¶

Deleted: ¶

Deleted: The use of GPR has allowed us to quickly

Deleted: (four days of fieldwork)

1 was an efficient compromise between spatial coverage and duration of the data acquisition (four days of fieldwork).
 2 On the other hand, the data processing was non-trivial, requiring about six months overall to set up an optimized
 3 workflow, due to challenging data characteristics, such as the steep and rugged topography and the sharp lateral
 4 variations of dielectrical properties of media (Triassic Dolostones vs Quaternary deposits).
 5 Our structural reconstruction derived by GPR data interpretation shows several sets of sub-vertical discontinuities
 6 within the near-surface (~ 1-4 m depth), which we interpreted as a pattern of extensional surface faulting. Such faults
 7 are bounding small local "graben or semi-graben-like" structures, which cut an hypothesized Holocene age clastic
 8 cover and underlying Triassic dolostones. We have also identified some chaotic and laterally discontinuous GPR-
 9 stratigraphic facies, interpreted as near-fault post-earthquake deposits (i.e. colluvial wedges?). These shallow
 10 structures suggest the possibility that surface faulting due to past strong earthquakes ($6 < M_w < 7$) occurred in relatively
 11 recent times in the study area. Its traces at surface were possibly later levelled by the concurrent natural processes of
 12 erosion, aggradation and, anthropogenic activities. As our results confirms the presence of seismic potential and thus
 13 the possible occurrence of a large earthquake in the future, we wish the primary effect of our study to be one of raising
 14 the level of attention regarding the seismic hazard in the Campotenese area, as well as prompting further research.
 15 Upon ground truthing, our work may represent a preparatory study for further geophysical surveys (3D GPR and other
 16 methods), as well as direct analysis including trenching, drilling, sampling campaigns and dating (e.g., luminescence,
 17 radiocarbon, etc). Although a further multidisciplinary approach would be necessary to achieve a quantitative (i.e. slip
 18 rates and recurrence times) assessment of the seismogenic potential of the study area, we firmly promote, particularly
 19 where near-surface data is lacking, a widespread use of the presented GPR workflow on other seismic gaps worldwide.

21 Acknowledgments

22 The study has benefited from several funding sources including: Agreement INGV-DPC 2012-2013 & 2014-2015,
 23 Project S1 – Miglioramento delle conoscenze per la definizione del potenziale sismogenetico - Base-knowledge
 24 improvement for assessing the seismogenic potential of Italy, <https://sites.google.com/site/ingvdpceprojects1/home>,
 25 resp. Cristina Pauselli, funded by Italian Presidenza del Consiglio dei Ministri – Dipartimento della Protezione Civile
 26 (DPC). The paper does not necessarily represent DPC official opinion and policy. We sincerely thank Leonardo
 27 Speziali, Prof. Costanzo Federico, and Roberto Volpe for their support during the field operations, as well as Khayal
 28 Gavarof for his valuable collaboration in data processing. We thank QGIS (<https://www.qgis.org/it/site/>) for providing
 29 the software with an open-source license, Petroleum Experts (<https://www.petex.com/products/move-suite/>), and dGB
 30 (<https://www.dgbes.com/>) for providing the academic licenses MOVE and OpenDtect software. We acknowledge
 31 NETGEO for academic access to the NRTK network (<http://www.netgeo.it/>). We would also like to thank the
 32 Ministero dell'Ambiente e della Tutela del Territorio e del Mare (MATTM) and the Regione Calabria for providing
 33 free access to geospatial data such as DTM and aerials (Regione Calabria - www.regione.calabria.it, under license
 34 IODL 2.0. - <https://www.dati.gov.it/iodl/2.0/>). The paper is the result of collaboration within the framework of the
 35 Interuniversity Center for 3D Seismotectonics with territorial applications - CRUST (<https://www.crust.unich.it/>). The
 36 GPR dataset presented in this study is available on request from the corresponding author.

Deleted: of the study site ...nd duration of the data acquisition (four days of fieldwork). On the other hands ...

Deleted: like th... such as the e...steep and rugged topography as well as ...

Deleted: geophysical

Deleted: More in detail of the study area, ...r structural reconstruction derived by GPR data interpretation shows several sets of sub-vertical discontinuities within the near-surface (~ 1-4 m depth range...), which we interpreted as a pattern of extensional extensional ...

Deleted: ,

Deleted: ,

Deleted: , hypothesized Holocene... down to...nd underlying Triassic dolostones, located within Holocene sediments and down to underlying dolostones... We have identified some chaotic and laterally discontinuous GPR-stratigraphic facies, interpreted as near-fault post-earthquake deposits (i.e. colluvial wedges ...). These shallow structures suggest the possibility that surface faulting due to past strong earthquakes ($6 < M_w < 7$) occurred in relatively recent times in the study area, but... I i...s traces at surface were possibly successively ...ater leveled...evelled ...y the concurrent natural processes of erosion, aggradation and, anthropogenic activities. All these buried features suggests that past strong earthquakes ($6 < M_w < 7$) might have occurred ...

Deleted: in the study area, which is located within the central sector of the well known "Mt. Pollino seismic gap".

Deleted: O...r resultsstudy...confirms the presence of seismic potential and thus the possible occurrence of a large earthquake in a ...

Deleted: As in the time range covered by the historical seismological catalogs there is no record of such energetic events, we hypothesize that the area could be at high risk of occurrence of a strong earthquake

Deleted: . ¶
W

Deleted: hope

Deleted: work ...study is to ...o be one of raising...the level of attention regarding the seismic hazard in the Campotenese area, thus ...

Deleted: to achieve an improvement of the base-knowledge for assessing its seismogenic potential

Deleted: We remark our GPR workflow doesn't allow to extract any date for events and neither identify a succession of past events. ...But u...on ground truthing, ...ur work may represent a preparatory study for further geophysical surveys (3D GPR and other methods), as well as direct analysis including for ...renching, drilling and... sampling campaigns and dating (e.g., ...dating via ...uminescence, radiocarbons... etc). Although a further multidisciplinary approach would be necessary to achieve a quantitative improvement ...i.e. slip rates and recurrence times) of the base-knowledge for assessing...ent of its...he seismogenic potential of the study area. ... wThus, w ...

Deleted: W

Deleted: more ...idespread use of the presented our ...PR workflow on other seismic gaps worldwide, ... particularly ...

Deleted: s

References

- Amicucci, L., Barchi, M.R., Montone, P., and Rubilani, N.: The Vallo di Diano and Auletta extensional basins in the southern Apennines (Italy): a simple model for a complex setting, *Terra Nova*, 20, 475-482, <https://doi.org/10.1111/j.1365-3121.2008.00841.x>, 2008.
- Amodio Morelli, L., Bonardi, G., Colonna, V., Dietrich, D., Giunta, G., Ippolito, F., Liguori, V., Lorenzoni, S., Paglionico, A., Perrone, V., Piccarreta, G., Russo, M., Scandone, P., Zanettin-Lorenzoni, E., and Zuppeta, A.: L'Arco calabro peloritano nell'orogene appenninico-maghrebide, *Mem. Soc. Geol. It.*, 17, 1-60, 1976.
- Anchuela, Ó.P., Lafuente, P., Arlegui, L., Liesa, C. L., and Simon, J. L.: Geophysical characterization of buried active faults: the Concud Fault (Iberian Chain, NE Spain), *Int J Earth Sci (Geol Rundsch)*, 105, 2221–2239, <https://doi.org/10.1007/s00531-015-1283-y>, 2016.
- Annan, A.P.: Ground-penetrating radar workshop notes, Sensors and Software Inc. Mississauga, ON, Canada, 192 pp., 2001.
- Ascione, A., Cinque, A., Santangelo, N., and Tozzi, M.: Il Bacino del Vallo di Diano e la tettonica trascorrente plio-quadernaria: nuovi vincoli cronologici e cinematici, *Stud. Geol. Camerti*, 1992/1, 201– 208, 1992a.
- Audru, J.C., Bano, M., Begg, J., Berryman, K., Henrys, S., and Niviere, B.: GPR investigations on active faults in urban areas: the Georisc-NZ project in Wellington, New Zealand, *Comptes Rendus de l'Academie des Sciences - Series IIA, Earth planet. Sci.*, 333(8), 447-454, [https://doi.org/10.1016/S1251-8050\(01\)01663-9](https://doi.org/10.1016/S1251-8050(01)01663-9), 2001.
- Bano, M., Edel, J.-B., Herquel G., and EPGS class 2001/2002: Geophysical investigation of a recent shallow fault, *The Leading Edge*, 21 (7), 648-650, <https://doi.org/10.1190/1.1497317>, 2002.
- Barchi, M.R., Lavecchia, G., Galadini, F., Messina P., Michetti, A. M., Peruzza, L., Pizzi, A., Tondi, E., and Vittori, E.: Sintesi delle conoscenze sulle faglie attive in Italia Centrale: parametrizzazione ai fini della caratterizzazione della pericolosità sismica, CNR-GNDT, Projects 5.1.2, 6a2, 5.1.1, Esagrafica, Roma, 2000.
- [Barchi, M.R., Carboni, F., Michele, M., Ercoli, M., Giorgetti, C., Porreca, M., Azzaro, S., Chiaraluce, L.: The influence of subsurface geology on the distribution of earthquakes during the 2016–2017 Central Italy seismic sequence, *Tectonophysics*, 807, 228797, <https://doi.org/10.1016/j.tecto.2021.228797>, 2021.](#)
- Bello S., de Nardis R., Scarpa R., Brozzetti F., Cirillo D., Ferrarini F., di Lieto B., Arrowsmith R. J., Lavecchia G.: Fault Pattern and Seismotectonic Style of the Campania – Lucania 1980 Earthquake (Mw 6.9, Southern Italy): New Multidisciplinary Constraints”, *Frontiers in Earth Science*, 8, 652, <https://doi.org/10.3389/feart.2020.608063>, 2021.
- Benson, A.K.: Applications of ground penetrating radar in assessing some geological hazards: examples of groundwater contamination, faults, cavities, *Journal of Applied Geophysics*, 33(1–3), 177–193, [https://doi.org/10.1016/0926-9851\(95\)90040-3](https://doi.org/10.1016/0926-9851(95)90040-3), 1995.
- Beres, M., Huggenberger, P., Green, A. G., and Horstmeyer, H.: Using two- and three-dimensional georadar methods to characterize glaciofluvial architecture, *Sediment. Geol.*, 129, 1-24, 1999.
- Boncio, P., Pizzi, A., Brozzetti, F., Pomposo, G., Lavecchia, G., Di Naccio, D., and Ferrarini, F., Coseismic ground deformation of the 6 april 2009 L'Aquila earthquake (central Italy, Mw 6.3), *Geoph. Res. Lett.*, 37, <http://dx.doi.org/10.1029/2010GL042807>, 2010.
- Brandes, C., Igel, J., Loewer, M., Tanner, D., C., Lang, J., Müller, K., and Winseman, J.: Visualisation and analysis of shear-deformation bands in unconsolidated Pleistocene sand using ground-penetrating radar: Implications for paleoseismological studies, *Sedimentary Geology*, 367, 135-145, <https://doi.org/10.1016/j.sedgeo.2018.02.005>, 2018.

1 Bricheva, S.S., Dubrovin, I.O., Lunina, O.V., Denisenko, I.A., Matasov, V.M., Turova, I.V., Entin, A.L., Panin, A.V.,
2 and Deev, E.V.: Numerical simulation of ground-penetrating radar data for studying the geometry of fault zone, Near
3 Surface Geophysics, Accepted Author Manuscript, <https://doi.org/10.1002/nsg.12153>, 2021.

4 Bristow, C.S., and Jol, H.M.: GPR in sediments: advice on data collection, basic processing and interpretation, a good
5 practice guide, In: Ground Penetrating Radar in Sediments, (Eds C.S. Bristow and H.M. Jol) Geol. Soc. Spec. Publ.,
6 211, 1-7, <https://doi.org/10.1144/GSL.SP.2001.211.01.02>, 2003.

7 Brozzetti, F., and Lavecchia, G.: Seismicity and related extensional stress field: the case of the Norcia Seismic Zone
8 (Central Italy), *Ann. Tectonicae*, 8(1), 36–57, 1994.

9 Brozzetti, F., Lavecchia, G., Mancini, G., Milana G., and Cardinali, M.: Analysis of the 9 September 1998 Mw 5.6
10 Mercure earthquake sequence (southern Apennines, Italy): a multidisciplinary approach, *Tectonophysics*, 476, 210-
11 225, <https://doi.org/10.1016/j.tecto.2008.12.007>, 2009.

12 Brozzetti, F.: The Campania-Lucania extensional fault system (southern Italy): a suggestion for a uniform model of
13 active extension in the Italian Apennines, *Tectonics*, 30 (5), 1-26, TC5009, <http://dx.doi.org/10.1029/2010TC002794>,
14 2011.

15 Brozzetti, F., Cirillo, D., de Nardis, R., Lavecchia, G., and Cardinali, M.: Detailed mapping of active faults in the
16 Calabro-Lucania Region, Report INGV-DPC 2014-2015 project S1 "Base-knowledge improvement for assessing the
17 seismogenic potential of Italy, <https://sites.google.com/site/ingvdp/projects1/home>, 2015.

18 Brozzetti, F., Cirillo, D., de Nardis, R., Cardinali, M., Lavecchia, G., Orecchio, B., Presti D., and Totaro, C.: Newly
19 identified active faults in the Pollino seismic gap, southern Italy, and their seismotectonic significance, *J. Struct. Geol.*,
20 94, 13-31, <https://doi.org/10.1016/j.jsg.2016.10.005>, 2017a.

21 Brozzetti, F., Cirillo, D., Liberi, F., Piluso, E., Faraca, E., De Nardis, R., and Lavecchia, G.: Structural style of
22 Quaternary extension in the Crati Valley (Calabrian Arc): Evidence in support of an east-dipping detachment fault, *It.*
23 *Journ. of Geosci.*, 136(3), 434-453, <https://doi.org/10.3301/IJG.2017.11>, 2017b.

24 Brozzetti, F., Boncio, P., Cirillo, D., Ferrarini, F., de Nardis, R., Testa, A., Liberi, F., and Lavecchia, G.: High
25 resolution field mapping and analysis of the August–October 2016 coseismic surface faulting (Central Italy
26 Earthquakes): slip distribution, parameterization and comparison with global earthquakes, *Tectonics*, 38, 417–439,
27 <https://doi.org/10.1029/2018TC005305>, 2019.

28 Brozzetti, F., Mondini, A.C., Pauselli, C., Mancinelli, P., Cirillo, D., Guzzetti, F., and Lavecchia, G.: Mainshock
29 anticipated by intra-sequence ground deformations: Insights from multiscale field and SAR interferometric
30 measurements, *Geosciences (Switzerland)*, 10(5), 186, <https://doi.org/10.3390/geosciences10050186>, 2020.

31 Bubeck, A., Wilkinson, M., Roberts, G.P., Cowie, P. A., McCaffrey, K.J.W., Phillips, R., and Sammonds, P.: The
32 tectonic geomorphology of bedrock scarps on active normal faults in the Italian Apennines mapped using combined
33 ground penetrating radar and terrestrial laser scanning, *Geomorphology*, 237, 38-51,
34 <https://doi.org/10.1016/j.geomorph.2014.03.011>, 2015.

35 Busby, J.P., and Merritt, J.W.: Quaternary deformation mapping with ground penetrating radar, *J. appl. Geophys.*,
36 41(1), 75–91, [https://doi.org/10.1016/S0926-9851\(98\)00050-.0](https://doi.org/10.1016/S0926-9851(98)00050-.0), 1999.

37 Cai, J., McMechan, G.A., and Fisher, M.A.: Application of ground penetrating radar to investigation of near-surface
38 fault properties in the San Francisco Bay region, *Bull. seism. Soc. Am.*, 86(5), 1459-1470, Available online: (accessed
39 09 feb 2021), <https://citeseerx.ist.psu.edu/viewdoc/download?doi=10.1.1.944.4417&rep=rep1&type=pdf>, 1996.

1 Calamita, F., Pizzi, A., and Roscioni, M.: I fasci di faglie recenti ed attive di M. Vettore - M. Bove e di M. Castello -
2 M. Cardosa (Appennino Umbro-Marchigiano), In *Studi Geologici Camerti*; Università di Camerino: Camerino, Italy,
3 1992; 81-95, Available online: <http://193.204.8.201:8080/jspui/handle/1336/552> (accessed on 09 Feb 2021), 1992.
4 Carpentier, S.F.A., Green, A.G., Langridge, R., Boschetti, S., Doetsch, J., Abacherli, A.N., Horstmeyer, H., and
5 Finnemore, M.: Flower structures and Riedel shears at a step over zone along the Alpine Fault (New Zealand) inferred
6 from 2-D and 3-D GPR images, *Journal Geophysical Research*, 117(B2), B02406,
7 <https://doi.org/10.1029/2011JB008749>, 2012a.
8 Carpentier, S.F.A., Green, A.G., Doetsch, J., Dorn, C., Kaiser, A.E., Campbell, F., Horstmeyer, H., and Finnemore,
9 M.: Recent deformation of Quaternary sediments as inferred from GPR images and shallow P-wave velocity
10 tomograms: Northwest Canterbury Plains, New Zealand, *J. Appl. Geophys.*, 8, 2-15,
11 <https://doi.org/10.1016/j.jappgeo.2011.09.007>, 2012b.
12 Cello G., E. Tondi, L. Micarelli, and L. Mattioni: Active tectonics and earthquake sources in the epicentral area of the
13 1857 Basilicata earthquake (southern Italy), *Journal of Geodynamics*, 36, 1–2, 37-50, [https://doi.org/10.1016/S0264-](https://doi.org/10.1016/S0264-3707(03)00037-1)
14 [3707\(03\)00037-1](https://doi.org/10.1016/S0264-3707(03)00037-1), 2003.
15 Chiaraluce, L., Di Stefano, R., Tinti, E., Scognamiglio, L., Michele, M., Casarotti, E., Cattaneo, M., De Gori, P.,
16 Chiarabba, C., Monachesi, G., Lombardi, A., Valoroso, L., Latorre, D., and Marzorati, S.: The 2016 Central Italy
17 Seismic Sequence: A First Look at the Mainshocks, Aftershocks, and Source Models, *Seismological Research Letters*,
18 88(3), 757-771, <https://doi.org/10.1785/0220160221>, 2017.
19 Christie, M., Tsoflas, G.P., Stockli, D.F., and Black, R.: Assessing fault displacement and off-fault deformation in an
20 extensional tectonic setting using 3-D ground-penetrating radar imaging, *J. appl. Geophys.*, 68(1), 9–16,
21 <https://doi.org/10.1016/j.jappgeo.2008.10.013>, 2009.
22 Cinti, F. R., Cucci, L., Pantosti, D., D'Addezio, G., and Meghraoui, M.: A major seismogenic fault in a 'silent area':
23 the Castrovillari fault (southern Apennines, Italy), *Geophysical Journal International*, 130(3), 595-605, Available
24 online: (accessed 09 Feb 2021), <https://www.earth-prints.org/bitstream/2122/12031/1/text.pdf>, 1997.
25 Cinti, F. R., Moro, M., Pantosti, D., Cucci, L., and D'Addezio, G.: New constraints on the seismic history of the
26 Castrovillari fault in the Pollino gap (Calabria, southern Italy), *J. Seismol.*, 6, 199-217,
27 <https://doi.org/10.1023/A:1015693127008>, 2002.
28 Cinti, F.R., Pauselli, C., Livio, F., Ercoli, M., Brunori, C.A., Ferrario, F., Volpe, R., Civico, R., Pantosti, D., Pinzi, S.,
29 De Martini, P.M., Ventura, G., Alfonsi, L., Gambillara, R., and Michetti, A.M.: Integrating multidisciplinary, multi-
30 scale geological and geophysical data to image the Castrovillari fault (Northern Calabria, Italy), *Geophys. J. Int.*, 203,
31 1847-1863, <https://doi.org/10.1093/gji/ggv404>, 2015a.
32 Cinti, F.R., L. Alfonsi, A. D'Alessio, S. Marino, C.A. Brunori: Faulting and Ancient Earthquakes at Sybaris
33 archaeological site, Ionian Calabria, Southern Italy, *Seism. Res. Lett.*, 86, 1, doi: 10.1785/02201401071, 2015b.
34 Cinti, F. R., De Martini, P. M., Pantosti, D., Baize, S., Smedile, A., Villani, F., et al.: 22-kyr-long record of surface
35 faulting along the source of the 30 October 2016 earthquake (central Apennines, Italy), from integrated paleoseismic
36 data sets. *Journal of Geophysical Research: Solid Earth*, 124, <https://doi.org/10.1029/2019JB017757>, 2019.
37 Cirillo, D., Totaro, C., Lavecchia, G., Orecchio, B., de Nardis, R., Presti, D., Ferrarini, F., Bello, S., and Brozzetti, F.:
38 Structural complexities and tectonic barriers controlling recent seismic activity of the Pollino area (Calabria-Lucania,
39 Southern Italy) – constraints from stress inversion and 3D fault model building, *Solid Earth Discuss. [preprint]*,
40 <https://doi.org/10.5194/se-2021-76>, in review, 2021.

Deleted: Cello, G., Deiana, G., Ferelli, L., Marchegiani, L., Maschio, L., Mazzoli, S., Michetti, A., Serva, L., Tondi, E., and Vittori, T.: Geological constraints for earthquake faulting studies in the Colfiorito area (Central Italy), *J. Seismol.*, 4, 357-364, <https://doi.org/10.1023/A:1026525302837>, 2000.¶

1 Cirillo, D.: Digital Field Mapping and Drone-Aided Survey for Structural Geological Data Collection and Seismic
2 Hazard Assessment: Case of the 2016 Central Italy Earthquakes, *Applied Sciences*, 10,
3 5233, <https://doi.org/10.3390/app10155233>, 2020.

4 Cirillo, D., Totaro, C., Lavecchia, G., Orecchio, B., de Nardis, R., Presti, D., Ferrarini, F., Bello, S., and Brozzetti, F.:
5 Structural complexities and tectonic barriers controlling recent seismic activity of the Pollino area (Calabria-Lucania,
6 Southern Italy) – constraints from stress inversion and 3D fault model building, [preprint of this special issue, Solid](https://doi.org/10.5194/se-2021-76)
7 [Earth](https://doi.org/10.5194/se-2021-76), <https://doi.org/10.5194/se-2021-76>, 2021.

8 Conyers, L.B.: *Ground-penetrating Radar for Geoarchaeology*, Wiley-Blackwell, London, Wiley Online Library, 160
9 pp., doi:10.1002/9781118949993, 2016.

10 Daniels, D. J., *Ground Penetrating Radar. Radar, Sonar and amp; Navigation*, Institution of Engineering and
11 Technology, London: IEE Press, 752 pp, <https://doi.org/10.1002/0471654507.emc152>, 2004.

12 Davis, J.L., and Annan, A.P.: Ground penetrating radar for high resolution mapping of soil and rock stratigraphy,
13 *Geophys. Prospect.*, 37, 531-551, 1989.

14 Demanet, F., Renardy, D., Vanneste, K., Jongmans, D., Camelbeeck, T., and Meghraoui, M.: The use of geophysical
15 prospecting for imaging active faults in the Roer Graben, Belgium, *Geophysics*, 66(1), 78–89,
16 <https://doi.org/10.1190/1.1444925>, 2001.

17 Dujardin, J. R., and Bano, M.: Topographic migration of GPR data: Examples from Chad and Mongolia, *Comptes*
18 *Rendus Geoscience*, 345, 2, 73-80, <https://doi.org/10.1016/j.crte.2013.01.003>, 2013.

19 Ercoli, M., Pauselli, C., Frigeri, A., Forte, E., and Federico, C.: “Geophysical paleoseismology” through high
20 resolution GPR data: A case of shallow faulting imaging in Central Italy, *Journal of Applied Geophysics*, 90, 27-40,
21 <https://doi.org/10.1016/j.jappgeo.2012.12.001>, 2013a.

22 Ercoli, M., Pauselli, C., Forte, E., Frigeri, A., and Federico, C.: The Mt. Pollino Fault (southern Apennines, Italy):
23 GPR signature of Holocene earthquakes in “silent” area, in: 7th Int. Work. Adv. Gr. Penetrating Radar, IEEE, 1–6,
24 <https://doi.org/10.1109/IWAGPR.2013.6601510>, 2013b.

25 Ercoli, M., Pauselli, C., Frigeri, A., Forte, E., and Federico, C.: 3-D GPR data analysis for high-resolution imaging of
26 shallow subsurface faults: The Mt Vettore case study (Central Apennines, Italy), *Geoph. J. Int.*, 198(1), 609-621,
27 <https://doi.org/10.1093/gji/ggu156>, 2014.

28 Ercoli, M., Pauselli, C., Cinti, F.R., Forte, E., and Volpe, R.: Imaging of an active fault: Comparison between 3D GPR
29 data and outcrops at the Castrovillari fault, Calabria, Italy, *Interpretation*, 3(3), SY57-SY66,
30 <https://doi.org/10.1190/INT-2014-0234.1>, 2015.

31 Ercoli, M., Di Matteo, L., Pauselli, C., Mancinelli, P., Frapiccini, S., Talegalli, L., and Cannata, A.: Integrated GPR
32 and laboratory water content measures of sandy soils: From laboratory to field scale, *Construction and Building*
33 *Materials*, 159,734-744, <https://doi.org/10.1016/j.conbuildmat.2017.11.082>, 2018.

34 Ercoli, M., Forte, E., Porreca, M., Carbonell, R., Pauselli, C., Minelli, G., and Barchi, M. R.: Using seismic attributes
35 in seismotectonic research: an application to the Norcia Mw = 6.5 earthquake (30 October 2016) in central Italy, *Solid*
36 *Earth*, 11, 329-348, <https://doi.org/10.5194/se-11-329-2020>, 2020.

37 [Ferrarini, F., de Nardis, R., Brozzetti, F., Cirillo, D., Arrowsmith, J. R. and Lavecchia, G.: Multiple Lines of Evidence](#)
38 [for a Potentially Seismogenic Fault Along the Central-Apennine \(Italy\) Active Extensional Belt–An Unexpected](#)
39 [Outcome of the MW6.5 Norcia 2016 Earthquake, *Front. Earth Sci.*, 9:642243, doi: 10.3389/feart.2021.642243, 2021.](#)

Deleted: submitted

Deleted: to

Deleted: 2021.

Deleted: Civico, R., Pucci, S., Villani, F., Pizzimenti, L., De Martini, P. M., Nappi, R., and the Open EMERGEIO Working Group: Surface ruptures following the 30 October 2016 Mw 6.5 Norcia earthquake, central Italy, *J. Maps*, 14, 151-160, <https://doi.org/10.1080/17445647.2018.1441756>, 2018.¶

Deleted: Conyers, L.B.: *Ground-penetrating Radar for Archaeological Mapping*. In: Wiseman J., El-Baz F. (eds) *Remote Sensing in Archaeology, Interdisciplinary Contributions To Archaeology*, Springer, New York, NY.

Deleted: https://doi.org/10.1007/0-387-44455-6_13

Deleted: , 2006.¶

Deleted: ¶
D’Agostino

1 [Ferrario, M. F., & Livio, F.: Characterizing the distributed faulting during the 30 October 2016, Central Italy](#)
2 [earthquake: A reference for fault displacement hazard assessment, *Tectonics*, 37,](#)
3 <https://doi.org/10.1029/2017TC004935>, 2018.

4 Filice, F., Liberi, F., Cirillo, D., Pandolfi, L., Marroni, M., and Piluso E.: Geology map of the central area of Catena
5 Costiera: insights into the tectono-metamorphic evolution of the Alpine belt in Northern Calabria, *Journal of Maps*,
6 11(1), 114-125, <https://doi.org/10.1080/17445647.2014.944877>, 2015.

7 Filice, F., and Seeber, L.: The Culmination of an Oblique Time-Transgressive Arc Continent Collision: The Pollino
8 Massif Between Calabria and the Southern Apennines, Italy, *Tectonics*, 38(1), 3261-3280,
9 <https://doi.org/10.1029/2017TC004932>, 2019.

10 Forte, E., and Pipan, M.: Review of multi-offset GPR applications: Data acquisition, processing and analysis, *Signal*
11 *Processing*, 132, 210-220, <https://doi.org/10.1016/j.sigpro.2016.04.011>, 2017.

12 Frigeri, A., and Ercoli, M.: The ScanMars Subsurface Radar Sounding Experiment on AMADEE-18, *Astrobiology*,
13 20(11), 1338-1352, <https://doi.org/10.1089/ast.2019.2037>, 2020.

14 Gafarov, K., Ercoli, M., Cirillo, D., Pauselli, C., and Brozzetti, F.: Extending surface geology data through GPR
15 prospections: Quaternary faulting signature from the Campotenese area (Calabria-Italy), 2018 17th International
16 Conference on Ground Penetrating Radar (GPR), Rapperswil, pp. 1-4, doi: 10.1109/ICGPR.2018.8441611, 2018.

17 [Galadini, F., C. Meletti, and E. Vittori: Major active faults in Italy: Available surficial data, *Netherlands J. Geosci.*](#)
18 [80, nos. 3/4, 273-296, 2001.](#)

19 Galadini, F., and Galli, P.: Paleoseismology of silent faults in the Central Apennines (Italy): the Mt. Vettore and Laga
20 Mts. Faults, *Annals of Geophysics*, 46(5), 815-836, <https://doi.org/10.4401/ag-3457>, 2003.

21 [Galli, P., Galderisi, A., Peronace, E., Giaccio, B., Hajdas, I., Messina, P., Pileggi, D., and Polpetta, F.: The awakening](#)
22 [of the dormant Mount Vettore fault \(2016 central Italy earthquake, Mw 6.6\): Paleoseismic clues on its millennial](#)
23 [silences, *Tectonics*, 38, 687-705, https://doi.org/10.1029/2018TC005326](#), 2019.

24 Galli, P.: Recurrence times of central-southern Apennine faults (Italy): Hints from paleoseismology, *Terra Nova*, 32,
25 399-407, <https://doi.org/10.1111/ter.12470>, 2020.

26 Geoportale Nazionale – Lidar data 1 m resolution, Ministero dell’Ambiente e della Tutela del Territorio e del Mare –
27 Creative Commons License (Cc BY-SA 3.0 IT), last access February 2018.

28 Ghisetti, F., and Vezzani, L.: Structural Map of Mt. Pollino (Southern Italy), 1:50.000 Scale, SELCA, Firenze, 1983.

29 Goodman, D., Hongo, H., Higashi, N., Inaoka, H., and Nishimura, Y.: GPR surveying over burial mounds: correcting
30 for topography and the tilt of the GPR antenna, *Near Surface Geophysics*, 5, 383-388, [https://doi.org/10.3997/1873-](https://doi.org/10.3997/1873-0604.2007020)
31 [0604.2007020](https://doi.org/10.3997/1873-0604.2007020), 2007.

32 Goodman, D., and Piro S.: GPR Remote Sensing in Archaeology Springer Science & Business Media (ISBN: 978–3–
33 642-31856-6), doi: 10.1007/978-3-642-31857-3, 2013.

34 Grandjaquet, C.L., and Grandjaquet, M.J.: Geologie de la zone de Diamante-Verbicaro (Calabre), *Geol. Romana* 1,
35 297-312, Available online: (accessed 09 Feb 2021), <http://www.dst.uniroma1.it/VolumeI>, 1962.

36 Grasmueck, M.: 3-D ground-penetrating radar applied to fracture imaging in gneiss, *Geophysics*, 61(4), 1050-1064,
37 <https://doi.org/10.1190/1.1444026>, 1996.

38 Grasmueck, M., Weger, R., and Horstmeyer, H.: Full-resolution 3D GPR imaging, *Geophysics*, 70(1), K12-K19,
39 2005.

Deleted: Galli, P., and Bosi, V.: Catastrophic 1638 earthquakes in Calabria (southern Italy): New insights from paleoseismological investigation. *J. Geophys. Res.*, 108, B12004, <https://doi.org/10.1029/2001JB001713>, 2003.¶

Deleted: Galli, P., Galadini, F., and Pantosti, D: Twenty years of paleoseismology in Italy, *Earth-Science Reviews*, 88(1-2), 89-117,

Deleted: <https://doi.org/10.1016/j.earscirev.2008.01.001>

Deleted: , 2008.¶

1 Green, A.G., Gross, R., Holliger, K., Horstmeyer, H., and Baldwin, J.: Results of 3-D georadar surveying and
2 trenching the San Andreas fault near its northern landward limit, *Tectonophysics*, 368, 7-23,
3 [https://doi.org/10.1016/S0040-1951\(03\)00147-1](https://doi.org/10.1016/S0040-1951(03)00147-1), 2003.

4 Gross, R., Green, A.G., Holliger, K., Horstmeyer, H., and Baldwin, J.: Shallow geometry and displacements on the
5 San Andreas Fault near Point Arena based on trenching and 3-D georadar surveying, *Geophysical Research Letters*,
6 29(20), 34-1-34-4, <https://doi.org/10.1029/2002GL015534>, 2002.

7 Gross, R., Green, A.G., Horstmeyer, H., Holliger, K., and Baldwin, J.: 3-D georadar images of an active fault: efficient
8 data acquisition, processing and interpretation strategies, *Subsurf. Sens. Technol. Appl.*, 4(1), 19-40,
9 <https://doi.org/10.1023/A:1023059329899>, 2003.

10 Gross, R., Green, A.G., Horstmeyer, H., and Begg, J.H.: Location and geometry of the Wellington Fault (New
11 Zealand) defined by detailed three-dimensional georadar data, *J. geophys. Res.*, 109, B05401,
12 <https://doi.org/10.1029/2003JB002615>, 2004.

13 Heincke, B., Green, A.G., van der Kruk, J., and Willenberg, H.: Semblance-based topographic migration (SBTM): A
14 method for identifying fracture zones in 3D georadar data, *Near Surface Geophysics*, 4(2), 79-88,
15 <https://doi.org/10.3997/1873-0604.2005034>, 2006.

16 Huggenberger, P.: Radar facies: recognition of facies patterns and heterogeneities within Pleistocene Rhine gravels,
17 NE Switzerland, In *Braided Rivers*, edited by J.L. Best and C.S. Bristow, *Geol. Soc. London Spec. Publ.*, 75, 163-
18 176, 1993.

19 Istituto Nazionale di Geofisica e Vulcanologia - INGV (2020 February, last access), <https://data.ingv.it/en/>.

20 Iannace, A., D'Errico, M., and Vitale, S.: Carta Geologica dell'area compresa tra Maratea, Castrovillari e Sangineto,
21 In: Vitale, S., Iannace, A. (Eds.), *Analisi Dello Strain Finito in 3D Dell'Unità Pollino-Ciagola (Confine Calabro-*
22 *lucano, Italia Meridionale)*, *Studi Geologici Camerti, Nuova Serie*, 2, 153-167 (ISSN: 0392-0631), 2004.

23 Iannace, A., Garcia Tortosa, F.J., and Vitale, S.: The Triassic metasedimentary successions across the boundary
24 between Southern Apennines and Calabria-Peloritani Arc (Northern Calabria, Italy), *Geol. J.*, 40, 155-171,
25 <https://doi.org/10.1002/gj.1001>, 2005.

26 Iannace, A., Vitale, S., D'Errico, M., Mazzoli, S., Di Staso, A., Macaione, E., Messina, A., Reddy, S.M., Somma, R.,
27 Zamparelli, V., Zattin, M., and Bonardi, G.: The carbonate tectonic units of northern Calabria (Italy): a record of
28 Apulian palaeomargin evolution and Miocene convergence, continental crust subduction, and exhumation of HP-LT
29 rocks, *J. Geol. Soc. Lond.*, 164, 1165-1186, <https://doi.org/10.1144/0016-76492007-017>, 2007.

30 Imposa, S., De Guidi, G., Grassi, S., Scudero, S., Barreca, G., Patti, G., and Boso, D.: Applying geophysical techniques
31 to investigate a segment of a creeping fault in the urban area of San Gregorio di Catania, southern flank of Mt. Etna
32 (Sicily - Italy), *Journal of Applied Geophysics*, 123, 153-163, <https://doi.org/10.1016/j.jappgeo.2015.10.008>, 2015.

33 ISIDe Working Group, Italian Seismological Instrumental and Parametric Database (ISIDe), Istituto Nazionale di
34 Geofisica e Vulcanologia (INGV), <https://doi.org/10.13127/ISIDE>, 2007.

35 Jewell, C.J., and Bristow, C.S.: GPR studies in the Piano di Pezza area of the Ovindoli-Pezza Fault, Central Apennines,
36 Italy: Extending palaeoseismic trench investigations with high resolution GPR profiling, *Near Surface Geophysics*,
37 4(3), 147-153, <https://doi.org/10.3997/1873-0604.2005040>, 2006.

38 Jol, H.M.: *Ground Penetrating Radar: Theory and Applications*, Elsevier, pp 544, ISBN: 9780444533487, 2009.

39 Lehmann, F., and Green, A.G.: Topographic migration of georadar data: Implications for acquisition and processing,
40 *Geophysics*, 65(3), 836-848, <https://doi.org/10.1190/1.1444781>, 2000.

Deleted: Gross, R., Holliger, K., Green, A.G., and John, B.: 3-D ground penetrating radar applied to paleoseismology: examples from the Wellington Fault, New Zealand, in *Proceedings of the Eighth International Conference on Ground Penetrating Radar*, 4084, 478-481, eds Noon, D.A., Stickley, G.F. & Longsta, D., Zurich, Switzerland, SPIE, <https://doi.org/10.1117/12.383615>, 2000.¶

Deleted: Guidoboni E., Ferrari G., Mariotti D., Comastri A., Tarabusi G., Sgattori G., and Valensise G.: CFTI5Med, *Catalogo dei Forti Terremoti in Italia (461 a.C.-1997) e nell'area Mediterranea (760 a.C.-1500)*, Istituto Nazionale di Geofisica e Vulcanologia (INGV), doi: <https://doi.org/10.6092/ingv.it-cfti5>, 2018.¶

Deleted: Horstmeyer, H., Corboz, P., Troncke, J., Nobes, D.C., Campbell, B.A., and Green, A.G.: High-resolution geophysical surveying at the Springfield Fault, New Zealand, in *Proceedings of the 11th European Meeting of Environmental and Engineering Geophysics, Near Surface 2005*, Palermo, Italy, 5-8 Sep. 2005, 4 pp., <https://doi.org/10.3997/2214-4609-pdb.13.P045>, 2005.¶

Deleted: Kagan, Y.Y., and Jackson, D.D.: Seismic Gap Hypothesis: Ten years after, *J. Geophys. Res.*, 96(B13), 21419-21431, <https://doi.org/10.1029/91JB02210>, 1991.¶

Leonard, M.: Earthquake fault scaling: Relating rupture length, width, average displacement, and moment release, *Bull. Seismol. Soc. Am.*, 100(5A), 1971-1988, <https://doi.org/10.1785/0120090189>, 2010.

Liberi, F., Morten, L., and Piluso, E.: Geodynamic significance of the ophiolites within the Calabrian Arc. *Island Arc*, 15, 26-43, <https://doi.org/10.1111/j.1440-1738.2006.00520.x>, 2006.

Liberty, L.M., Hemphill-Haley, M.A., and Madin, I.P.: The Portland Hills Fault: uncovering a hidden fault in Portland, Oregon using high resolution geophysical methods, *Tectonophysics*, 368(1-4), 89-103, [https://doi.org/10.1016/S0040-1951\(03\)00152-5](https://doi.org/10.1016/S0040-1951(03)00152-5), 2003.

Liner, C.L., and Liner, J.L.: Application of GPR to a site investigation involving shallow faults, *The Leading Edge*, 16(11), 1649-1651, <https://doi.org/10.1190/1.1437545>, 1997.

Malik, J.N., Sahoo, A.K., and Shah, A.A.: Ground-penetrating radar investigation along Pinjore Garden Fault: implication toward identification of shallow subsurface deformation along active fault, NW Himalaya, *Curr. Sci.*, 93(10), 1422-1427, 2007.

Malik, J. N., Kumar, A., Satuluri, S., Puhan, B., and Mohanty, A.: Ground-Penetrating Radar Investigations along Hajipur Fault: Himalayan Frontal Thrust-Attempt to Identify Near Subsurface Displacement, NW Himalaya, India", *International Journal of Geophysics*, Article ID 608269, 7 pp., <https://doi.org/10.1155/2012/608269>, 2012.

Maschio, L., Ferranti, L., and Burrato, P.: Active extension in Val d'Agri area, southern Apennines, Italy: Implications for the geometry of the seismogenic belt, *Geophys. J. Int.*, 162, 591-609, <https://doi.org/10.1111/j.1365-246X.2005.02597.x>, 2005.

Matoš, B., Zajc, M., Kordić, B., Tomljenović, B., and Gosar, A.: Quaternary fault activity in the SW Pannonian Basin: GPR surveying in the Bilogora Mt. (NE Croatia), *Geological Quarterly*, 61(1), 18-36, doi: <https://doi.org/10.7306/gq.1308>, 2017.

McCalpin, J.P.: *Paleoseismology*, 2nd Edition, International Geophysics Series, 95, Elsevier Publishing, 647 pp., plus additional website content at: www.elsevier.com, ISBN 978-0-12-373576-8, 2009.

McCann, W.R., Nishenko, S.P., Sykes, I.R., and Krause, J.: Seismic gaps and plate tectonics: seismic potential for major boundaries, *Pure and applied geophysics*, 117, 1082-1147, 1979.

McClymont, A.F., Green, A.G., Villamor, P., Horstmeyer, H., Grass, C., and Nobes, D.C.: Characterization of the shallow structures of active fault zones using 3-D GPR data, *J. geophys. Res.*, 113, B10315, <https://doi.org/10.1029/2007JB005402>, 2008.

McClymont, A.F., Villamor, P., and Green, A.G.: Fault displacement accumulation and slip rate variability within the Taupo Rift (New Zealand) based on trench and 3-D ground-penetrating radar data, *Tectonics*, 28, TC4005, <https://doi.org/10.1029/2008TC002334>, 2009.

McClymont, A.F., Green, A.G., Kaiser, A., Horstmeyer, H., and Langridge, R.: Shallow fault segmentation of the Alpine fault zone, New Zealand revealed from 2- and 3-D GPR surveying, *J. Appl. Geophys.*, 70(4), 343-354, <https://doi.org/10.1016/j.jappgeo.2009.08.003>, 2010.

Michele, M., Chiaraluce, L., Di Stefano, R., & Waldhauser, F.: Fine-scale structure of the 2016-2017 Central Italy seismic sequence from data recorded at the Italian National Network. *Journal of Geophysical Research: Solid Earth*, 125, e2019JB018440, <https://doi.org/10.1029/2019JB018440>, 2020.

Michetti, A. M., Ferrelì, L., Serva, L., and Vittori, E.: Geological evidence for strong historical earthquakes in an "aseismic" region: The Pollino case (Southern Italy), *Journal of Geodynamics*, 24:1-4, 67-86, [https://doi.org/10.1016/S0264-3707\(97\)00018-5](https://doi.org/10.1016/S0264-3707(97)00018-5), 1997.

1 Michetti, A. M., Ferrel, L., Esposito, E., Porfido, S., Blumetti, A. M., Vittori, E., Serva, L., and Roberts, G. P.: Ground
2 Effects during the 9 September 1998, Mw = 5.6 Lauria, Earthquake and the Seismic Potential of the seismic Pollino
3 Region in Southern Italy, *Seismological Research Letters*, 71(1), 31-46, <https://doi.org/10.1785/gssrl.71.1.31>, 2000.

4 Mogi K.: Two Kinds of Seismic Gaps. In: Wyss M. (eds) *Earthquake Prediction and Seismicity Patterns*, Contributions
5 to Current Research in Geophysics, Birkhäuser, Basel, https://doi.org/10.1007/978-3-0348-6430-5_4, 1979.

6 Napolitano, F., De Siena, L., Gervasi, A., Guerra, I., Scarpa, R., and La Rocca, M.: Scattering and absorption imaging
7 of a highly fractured fluid-filled seismogenic volume in a region of slow deformation, *Geosci. Front.*, 11(3), 989-
8 998, <https://doi.org/10.1016/j.gsf.2019.09.014>, 2020.

9 Napolitano, F., Galluzzo, D., Gervasi, A., Scarpa, R., and La Rocca, M.: Fault imaging at Mt Pollino (Italy) from
10 relative location of microearthquakes, *Geophysical Journal International*, 224(1), 637-
11 648, <https://doi.org/10.1093/gji/ggaa407>, 2021.

12 Nobes, D. C., Jol, H. M., and Duffy, B.: Geophysical imaging of disrupted coastal dune stratigraphy and possible
13 mechanisms, Haast, South Westland, New Zealand, *New Zealand Journal of Geology and Geophysics*, 59:3, 426-435,
14 doi: 10.1080/00288306.2016.1168455, 2016.

15 Oddone, E.: Gli elementi fisici del grande terremoto marsicano-fucense del 13 gennaio 1915. *Boll. Soc. Sismol. Ital.*
16 *19*, 71-216, 1915

17 Ogniben, L.: Schema introduttivo alla geologia del confine calabro-lucano, *Mem. Soc. Geol. It.*, 8, 453-763, 1969.

18 Overgaard, T. and Jakobsen, P.R.: Mapping of glaciotectionic deformation in an ice marginal environment with ground
19 penetrating radar, *Journal Applied Geophysics*, 47(3-4), 191-197, [https://doi.org/10.1016/S0926-9851\(01\)00064-7](https://doi.org/10.1016/S0926-9851(01)00064-7),
20 2001.

21 Passarelli, L., Hainzl, S., Cesca, S., Maccaferri, F., Mucciarelli, M., Roessler, D., Corbi, F., Dahm, T., Rivalta, E.:
22 Aseismic transient driving the swarm-like seismic sequence in the Pollino range, Southern Italy, *Geophysical Journal*
23 *International*, 201:3, 1553-1567, <https://doi.org/10.1093/gji/ggv111>, 2015.

24 Pantosti, D. and Valensise, G.: Faulting mechanism and complexity of the November 23, 1980, Campania-Lucania
25 earthquake, inferred from surface observations, *J. Geophys. Res.*, 95(B10), 15,319-15,341,
26 <https://doi.org/10.1029/JB095iB10p15319>, 1990.

27 Pastori, M., Margheriti, L., De Gori, P., Govoni, A., Lucente, F.P., Moretti, M., Marchetti, A., Di Giovambattista, R.,
28 Anselmi, M., De Luca, P., Nardi, A., Agostinetti, N.P., Latorre, D., Piccinini, D., Passarelli, L., and Chiarabba, C.:
29 The 2011-2014 Pollino Seismic Swarm: Complex Fault Systems Imaged by 1D Refined Location and Shear Wave
30 Splitting Analysis at the Apennines-Calabrian Arc Boundary, *Front. Earth Sci.*, 9:618293, doi:
31 10.3389/feart.2021.618293, 2021.

32 Patacca, E. and Scandone, P.: Geological interpretation of the CROP-04 seismic line (Southern Apennines, Italy),
33 *Boll. Soc. Geol. It. (Ital. J. Geosci.)*, 7, 297-315, 2007.

34 Pauselli, C., Federico, C., Frigeri, A., Orosei, R., Barchi, M.R., and Basile, G.: Ground Penetrating Radar
35 investigations to study active faults in the Norcia Basin (Central Italy), *J. Appl. Geophys.*, 72, 39-45,
36 <https://doi.org/10.1016/j.jappgeo.2010.06.009>, 2010.

37 Pauselli, C., Ercoli, M., Volpe, R., Federico, C., Mazzocca, M., and Speziali, L.: 2D and 3D GPR images of selected
38 fault planes (Calabro-Lucania border), Report DPC-INGV-S1 Project "Base-knowledge improvement for assessing
39 the seismogenic potential of Italy", deliverable D18/c1.1 - (<https://sites.google.com/site/ingvdpcprojects1/documents>,
40 Agreement INGV-DPC 2014-2015), 49 pp., 2015.

Deleted: <https://sites.google.com/site/ingvdpcprojects1/home>


1 Plafker, G. and Galloway, J. P.: Lessons Learned from the Lorna Prieta, California, Earthquake of October 17, 1989,
2 USGS Numbered Series Circular 1045, 48 pp., <https://doi.org/10.3133/cir1045>, 1989.

3 Pondrelli, S., Salimbeni, S., Ekström, G., Morelli, A., Gasperini, P., and Vannucci, P.: The Italian CMT dataset from
4 1977 to present, Phys. Earth Plan. Int., 159, 286-303, 2006.

5 Porreca, M., Minelli, G., Ercoli, M., Brobia, A., Mancinelli, P., Cruciani, F., Giorgetti, C., Carboni, F., Mirabella, F.,
6 Cavinato, G., Cannata, A., Pauselli, C., and Barchi, M.R.: Seismic reflection profiles and subsurface geology of the
7 area interested by the 2016-2017 earthquake sequence (Central Italy), in: The 2016 Central Italy Seismic Sequence:
8 Insights, implications and lessons learned, *Tectonics*, 37, 1116-1137, <https://doi.org/10.1002/2017TC004915>, 2018.

9 Porreca, M., Fabbri, A., Azzaro, S., Pucci, S., Del Rio, L., Pierantoni, P. P., Giorgetti, C., Roberts, G., Barchi,
10 M.R.: 3D geological reconstruction of the M. Vettore seismogenic fault system (Central Apennines, Italy): Cross-
11 cutting relationship with the M. Sibillini thrust, Journal of Structural Geology, 131, 103938,
12 <https://doi.org/10.1016/j.jsg.2019.103938>, 2020.

13 Pousse-Beltran, L., Vassallo, R., Audemard, F., Jouanne, F., Oropeza, J., Garambois, S., and Aray, J.: Earthquake
14 geology of the last millennium along the Boconó Fault, Venezuela, *Tectonophysics*, 747-748, 40-53,
15 <https://doi.org/10.1016/j.tecto.2018.09.010>, 2018.

16 Pucci, S., Pizzimenti, L., Civico, R., Villani, F., Brunori, C.A., Pantosti, D.: High resolution morphometric analysis
17 of the Cordone del Vettore normal fault scarp (2016 central Italy seismic sequence): Insights into age, earthquake
18 recurrence and throw rates, Geomorphology, 388, <https://doi.org/10.1016/j.geomorph.2021.107784>, 2021.

19 Quitow, H. W.: Der Deckenbau des Kalabrischen Massivs und seiner Rangebiete. Beitr. geol. Westl.
20 Mediterrangebiete Abh. Ges. Wiss. Göttingen, Math.-Phis. Kl. s. 3, 13: 63-179, 1935.

21 Reiss, S., Reicherter, K. R., and Reuther, C. D.: Visualization and characterization of active normal faults and
22 associated sediments by high-resolution GPR Geological Society, London, Special Publications, 211, 247-255,
23 doi:10.1144/GSL.SP.2001.211.01.20, 2003.

24 Roberts, G.P., Raithatha, B., Sileo, G., Pizzi, A., Pucci, S., Walker, J.F., et al.: Shallow subsurface structure of the
25 2009 April 6 Mw 6.3 L'Aquila earthquake surface rupture at Paganica, investigated with ground-penetrating radar,
26 *Geophys. J. Int.*, 183(2), 774-790, <https://doi.org/10.1111/j.1365-246X.2010.04713.x>, 2010.

27 Rovida, A., Locati, M., Camassi, R., Lolli, B., and Gasperini, P.: The Italian earthquake catalogue CPTI15, Bulletin
28 of Earthquake Engineering, 18, 2953-2984, <https://doi.org/10.1007/s10518-020-00818-y>, 2020.

29 Salvi, S., Cinti, F.R., Colini, L., D'Addezio, G., Doumaz, F., and Pettinelli, E., Investigation of the active Celano-
30 L'Aquila fault system, Abruzzi (central Apennines, Italy) with combined ground-penetrating radar and palaeoseismic
31 trenching, *Geophys. J. Int.*, 155(3), 805-818, <https://doi.org/10.1111/j.1365-246X.2003.02078.x>, 2003.

32 Sangree, J., B. and Widmier, J. M.: Interpretation of depositional facies from seismic data, *Geophysics*, 44, 131-60,
33 <https://doi.org/10.1190/1.1440957>, 1979.

34 Sapia, V., Villani, F., Fischanger, F., Lupi, M., Baccheschi, P., Pantosti, D., et al.: 3-D deep electrical resistivity
35 tomography of the major basin related to the 2016 Mw 6.5 central Italy earthquake fault. Tectonics, 40,
36 e2020TC006628, <https://doi.org/10.1029/2020TC006628>, 2021.

37 Schiattarella, M., Torrente, M., and Russo, F.: Analisi strutturale ed osservazioni morfotettoniche nel bacino del
38 Mercure (Confine calabro-lucano), *Il Quaternario*, 7, 613-626, 1994.

39 Scognamiglio, L., Tinti, E., and Quintiliani, M.: Time Domain Moment Tensor (TDMT) [Data set], Istituto Nazionale
40 di Geofisica e Vulcanologia (INGV), <https://doi.org/10.13127/TDMT>, <http://terremoti.ingv.it/tdmt>, 2006.

Deleted: Pondrelli, S.: European-Mediterranean Regional Centroid-Moment Tensors Catalog (RCMT) [Data set], Istituto Nazionale di Geofisica e Vulcanologia (INGV), <https://doi.org/10.13127/rcmt/euromed>, <http://rcmt2.bo.ingv.it/>, 2002.¶

Deleted: Pucci, S., De Martini, P. M., Civico, R., Villani, F., Nappi, R., Ricci, T. et al., and Pantosti, D.: Coseismic ruptures of the 24 August 2016, Mw 6.0 Amatrice earthquake (central Italy), *Geophysical Research Letters*, 44, 2138-2147, <https://doi.org/10.1002/2016GL071859>, 2017.¶

Deleted: Quitow, H.W.: Derdeckenbaudes Kalabrischenmassivs und seiner Randgebiete, Abh. Ges. Wiss. Göttingen, Math Phys. Kl., 13, 63-179, 1935.¶

Deleted: ¶

1 Servizio Geologico d'Italia: 220 Verbicaro and 221 Castrovillari Sheets of the Carta Geologica D'Italia, 1. 100.000
2 Scale, Rome, 1970.

3 Shaikh, M.A., Maurya, D.M., Mukherjee, S., Vanik, N.P., Padmalal, A., and Chamyal, L.S.: Tectonic evolution of the
4 intra-uplift Vigodi-Gugriana-Khirsara-Netra Fault System in the seismically active Kachhh rift basin, India:
5 Implications for the western continental margin of the Indian plate, *Journal of Structural Geology*, 140, 104124,
6 <https://doi.org/10.1016/j.jsg.2020.104124>, 2020.

7 Sketsiou, P., De Siena, L., Gabrielli, S., Napolitano, F., 3-D attenuation image of fluid storage and tectonic interactions
8 across the Pollino fault network, *Geophysical Journal International*, 226:1, 536–547,
9 <https://doi.org/10.1093/gji/ggab109>

10 Slater, L. and Niemi, T.M.: Ground-penetrating radar investigation of active faults along the Dead Sea Transform and
11 implications for seismic hazards within the city of Aqaba, Jordan, *Tectonophysics*, 368(1-4), 33-50,
12 [https://doi.org/10.1016/S0040-1951\(03\)00149-5](https://doi.org/10.1016/S0040-1951(03)00149-5), 2003.

13 Smith, D. G. and Jol, H. M.: Wasatch fault (Utah), detected and displacement characterized by ground penetrating
14 radar, *Environ. Eng. Geosci.*, 1, 489-496, 1995.

15 Spina, V., Galli, P., Tondi, E., and Mazzoli, S.: Fault propagation in a seismic gap area (northern Calabria, Italy):
16 implications for seismic hazard, *Tectonophysics*, 476, 357-369, 2009.

17 Stirling, M., Goned, T., Berryman, K., and Litchfield, N.: Selection of Earthquake Scaling Relationships for Seismic-
18 Hazard Analysis, *Bulletin of the Seismological Society of America*, 103(6), 2993-
19 3011, <https://doi.org/10.1785/0120130052>, 2013.

20 Tangari, A.C., Scarciglia, F., Piluso, E., Marinangeli, L., and Pompilio, L.: Role of weathering of pillow basalt,
21 pyroclastic input and geomorphic processes on the genesis of the Monte Cerviero upland soils (Calabria, Italy), *Catena*,
22 171, 299-315, ISSN 0341-8162, <https://doi.org/10.1016/j.catena.2018.07.015>, 2018.

23 Tarquini, S., Vinci, S., Favalli, M., Doumaz, F., Fornaciai, A. and Nannipieri, L.: Release of a 10-m-resolution DEM
24 for the Italian territory: Comparison with global-coverage DEMs and anaglyph-mode exploration via the web,
25 *Computers & Geosciences*, 38, 168-170, <https://doi.org/10.1016/j.cageo.2011.04.018>, 2012.

26 Tertulliani A. and Cucci, L.: New insights on the strongest historical earthquake in the Pollino region (southern Italy),
27 *Seismol. Res. Lett.*, 85(3), 743-751, <https://doi.org/10.1785/0220130217>, 2014.

28 Testa, A., Boncio, P., Di Donato, M., Mataloni, G., Brozzetti, F., and Cirillo, D.: Mapping the geology of the 2016
29 Central Italy earthquake fault (Mt. Vettore – Mt. Bove fault, Sibillini Mts.): geological details on the Cupi – Ussita
30 and Mt. Bove - Mt. Porche segments and overall pattern of coseismic surface faulting, *Geological Field Trips and*
31 *Maps, Italian Geological Society and of the Geological Survey of Italy*, 11(2.1), 1-13,
32 <https://doi.org/10.3301/GFT.2019.03>, 2019.

33 Tortorici, L., Monaco, C., Tansi, C., and Cocina, O.: Recent and active tectonics in the Calabrian arc (Southern Italy),
34 *Tectonophysics*, 243(1-2), pp. 37–55, [https://doi.org/10.1016/0040-1951\(94\)00190-K](https://doi.org/10.1016/0040-1951(94)00190-K), 1995.

35 Totaro, C., Koulakov, I., Orecchio, B., and Presti, D.: Detailed crustal structure in the area of the southern Apennines–
36 Calabrian Arc border from local earthquake tomography, *J. Geodyn.*, 82, 87-97,
37 <https://doi.org/10.1016/j.jog.2014.07.004>, 2014.

38 Totaro, C., Seeber, L., Waldhauser, F., Steckler, M., Gervasi, A., Guerra, I., Orecchio, B., and Presti, D.: An intense
39 earthquake swarm in the southernmost Apennines: fault architecture from high-resolution hypocenters and focal
40 mechanisms, *Bull. Seismol. Soc. Am.* 105, 1-6, <https://doi.org/10.1785/0120150074>, 2015.

Tronicke, J., Villamor, P., and Green, A. G.: Detailed shallow geometry and vertical displacement estimates of the Maleme Fault Zone, New Zealand, using 2D and 3D georadar, *Near Surface Geophysics*, 4(3), 155-161, <https://doi.org/10.3997/1873-0604.2005041>, 2006.

Utzi, E. C.: *Ground Penetrating Radar*, Elsevier, 209 pp., <http://dx.doi.org/10.1016/B978-0-08-102216-0.00001-1>, 2017.

Wallace, S. C., Nobes, D. C., Davis, K. J., Burbank, D. W., and White, A.: Three-dimensional GPR imaging of the Benmore anticline and step-over of the Ostler Fault, South Island, New Zealand, *Geophysical Journal International*, 180(2), 465-474, <https://doi.org/10.1111/j.1365-246X.2009.04400.x>, 2010.

Vanneste, K., Verbeeck, K., and Petermans, T.: Pseudo-3-D imaging of a low-slip-rate, active normal fault using shallow geophysical methods: the Geleen fault in the Belgian Mass River valley, *Geophysics*, 73(1), B1-B9, <https://doi.org/10.1190/1.2816428>, 2008.

Wells, D.L. and Coppersmith, K.J.: New empirical relationships among magnitude, rupture length, rupture width, rupture area, and surface displacement, *Bull. Seismol. Soc. Am.*, 84(4), 974-1002, 1994.

Wesnowsky, S.G.: Displacement and geometrical characteristics of earthquake surface ruptures: Issues and implications for seismic hazard analysis and the process of earthquake rupture, *Bull. Seismol. Soc. Am.*, 98(4), 1609-1632, <https://doi.org/10.1785/0120070111>, 2008.

Vezzani, L., Festa, A., and Ghisetti, F.C.: Geology and tectonic evolution of the Central-Southern Apennines, Italy, *Special Paper of the Geological Society of America*, 469, 1-58, <https://doi.org/10.1130/SPE469>, 2010.

Villani, F. and Pierdominici, S.: Late Quaternary tectonics of the Vallo di Diano basin (southern Apennines, Italy), *Quat. Sci. Rev.*, 29, 3167-3183, <https://doi.org/10.1016/j.quascirev.2010.07.003>, 2010.

Villani, F., Pucci, S., Civico, R., De Martini, P. M., Cinti, F. R., and Pantosti, D.: Surface faulting of the 30 October 2016 Mw 6.5 central Italy earthquake: Detailed analysis of a complex coseismic rupture, *Tectonics*, 37, 3378-3410, <https://doi.org/10.1029/2018TC005175>, 2018.

Villani, F., Maraio, S., Bruno, P. P., Improta, L., Wood, K., Pucci, S., et al.: High-resolution seismic profiling in the hanging wall of the southern fault section ruptured during the 2016 Mw 6.5 central Italy earthquake. *Tectonics*, 40, e2021TC006786, <https://doi.org/10.1029/2021TC006786>, 2021.

Yalciner, C.C., Altunel, E., Bano, M., Meghraoui, M., Karabacak, V., and Akyuz, H. S.: Application of GPR to normal faults in the Büyük Menderes Graben, Western Turkey, *Journal of Geodynamics*, 65, 218-227, <https://doi.org/10.1016/j.jog.2012.05.011>, 2013.

Zajc, M., Celarc, B., and Gosar, A.: GPR Study of a Thrust-Fault in an Active Limestone Quarry (SW Slovenia), *JEEG*, 23(4), 457-468: <https://doi.org/10.2113/JEEG23.4.457>, 2018.

Zhang, D., Li, J., Liu, S., and Wang, G.: Multi-frequencies GPR measurements for delineating the shallow subsurface features of the Yushu strike slip fault, *Acta Geophys.*, 67, 501-515, <https://doi.org/10.1007/s11600-019-00271-9>, 2019.

Deleted: Vittori, E., Deiana, G., Esposito, E., Ferrel, L., Marchegiani, L., Mastrolorenzo, G., Michetti, A.M., Porfido, S., Serva, L., Simonelli, A.L., and Tondi, E.: Ground effects and surface faulting in the September-October 1997 Umbria-Marche (Central Italy) seismic sequence, *J. Geodyn.*, 29, 535-564, [https://doi.org/10.1016/S0264-3707\(99\)00056-3](https://doi.org/10.1016/S0264-3707(99)00056-3), 2000.¶

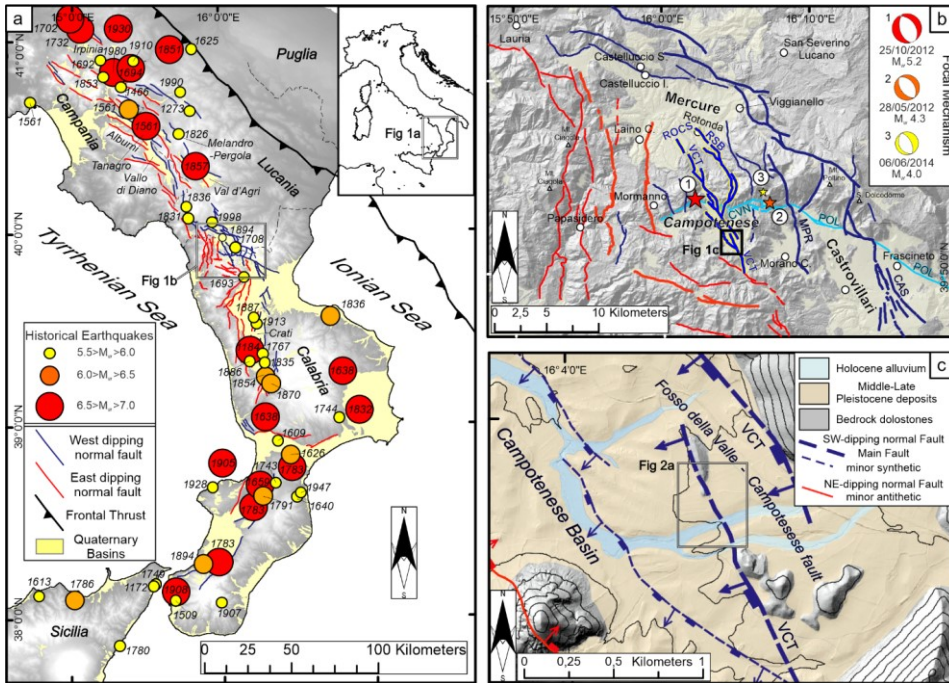


Figure 1

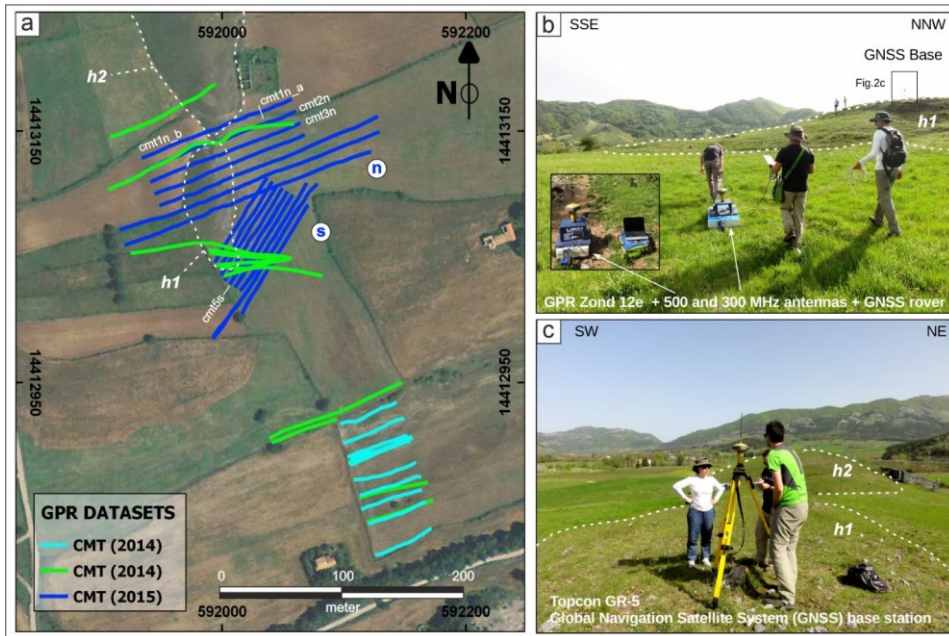


Figure 2

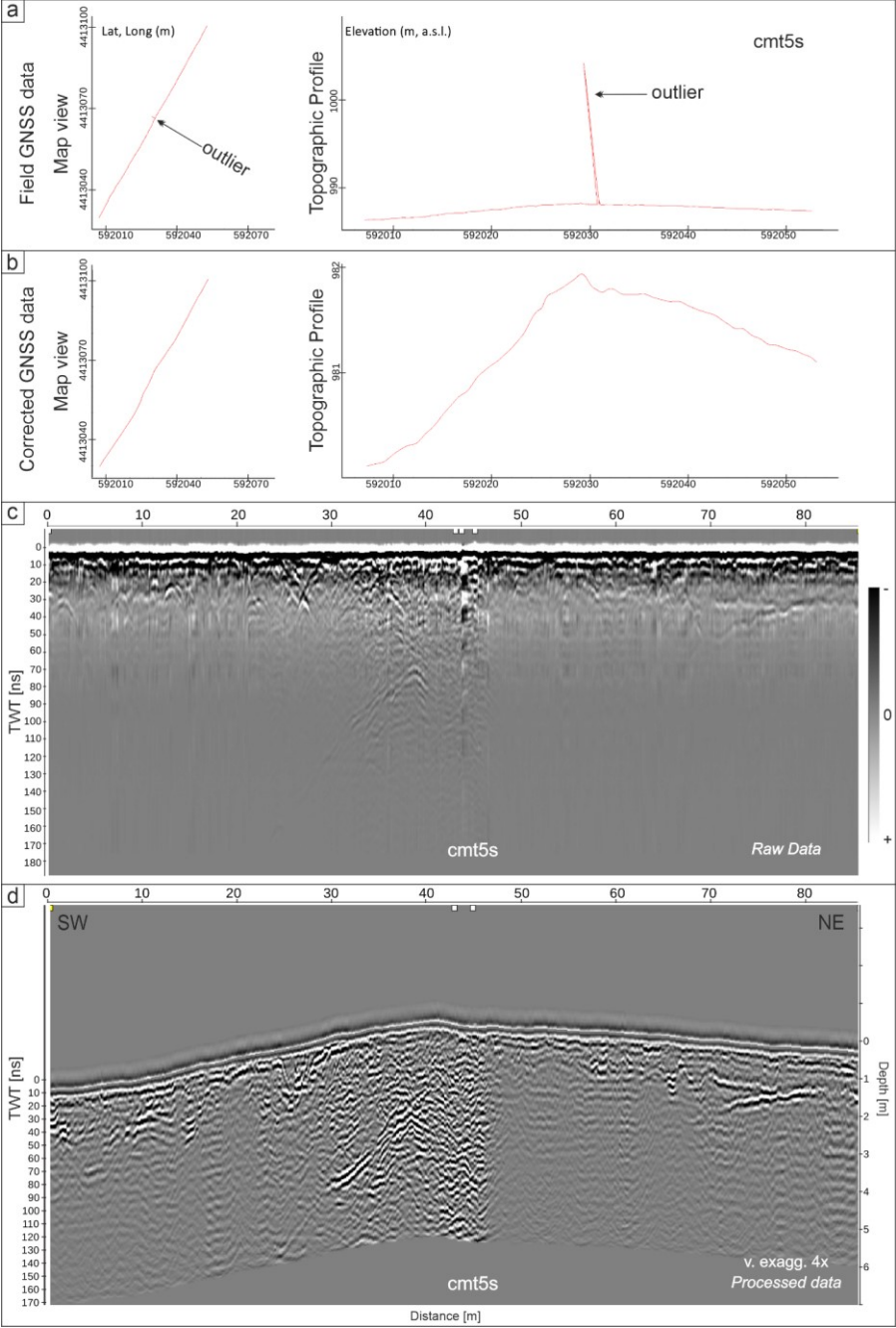


Figure 3

1
2

3
4
5

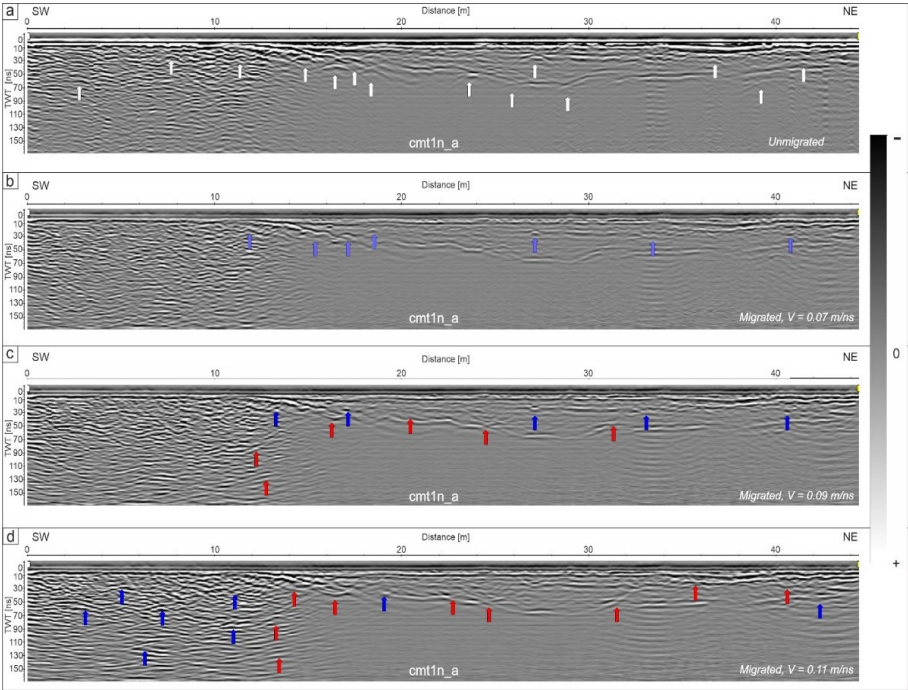


Figure 4

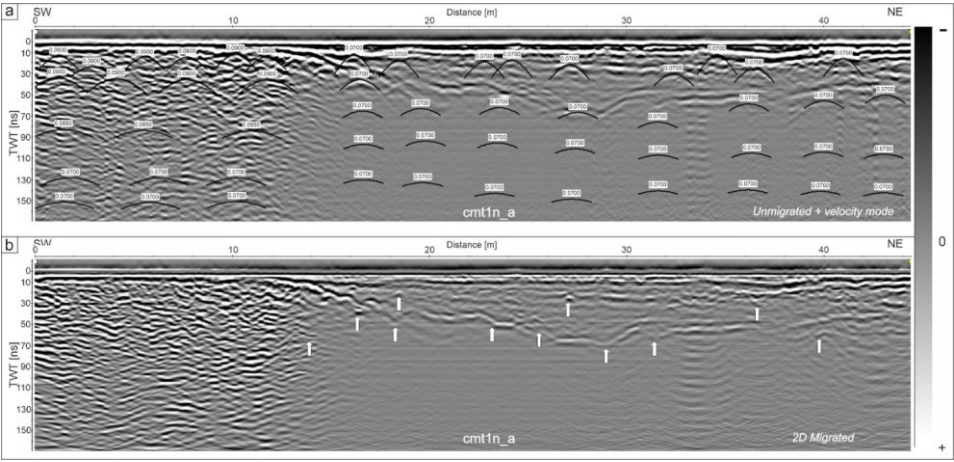


Figure 5

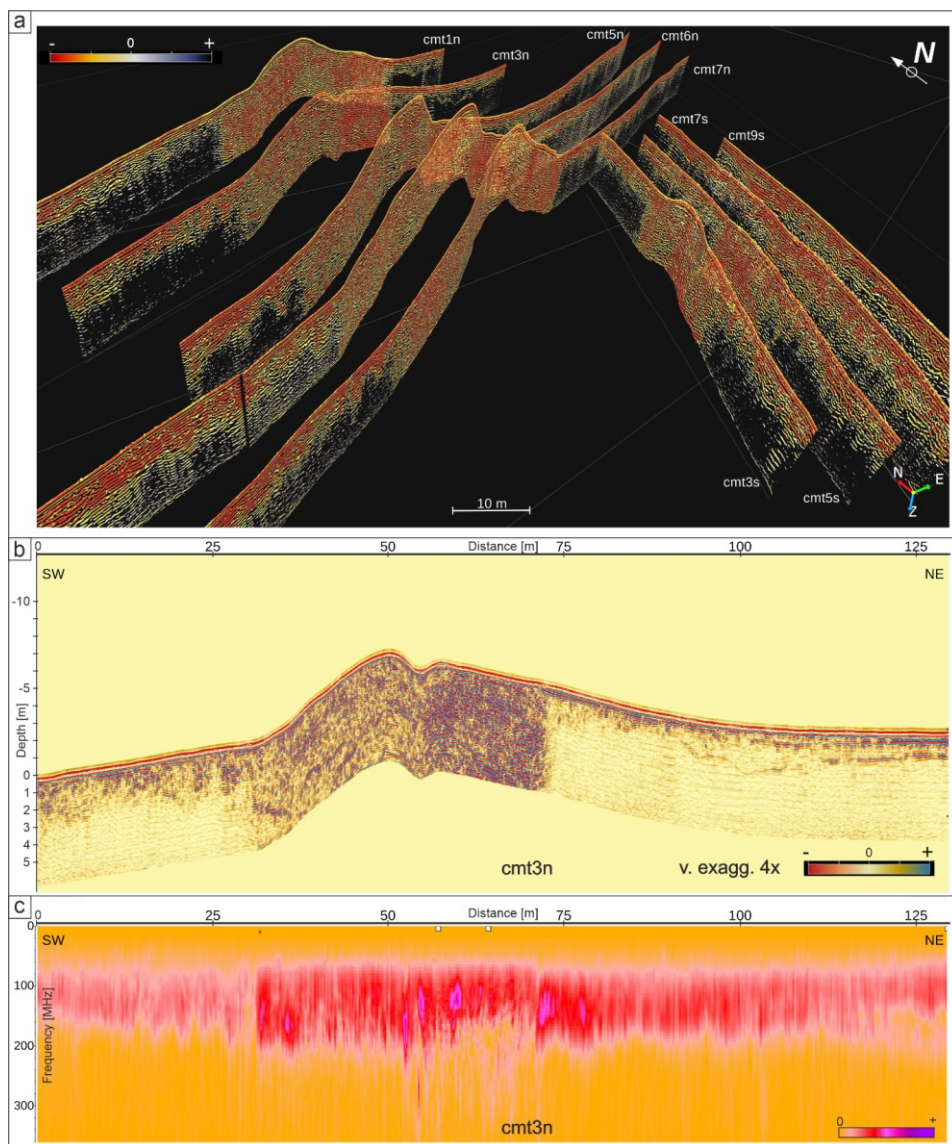


Figure 6

1

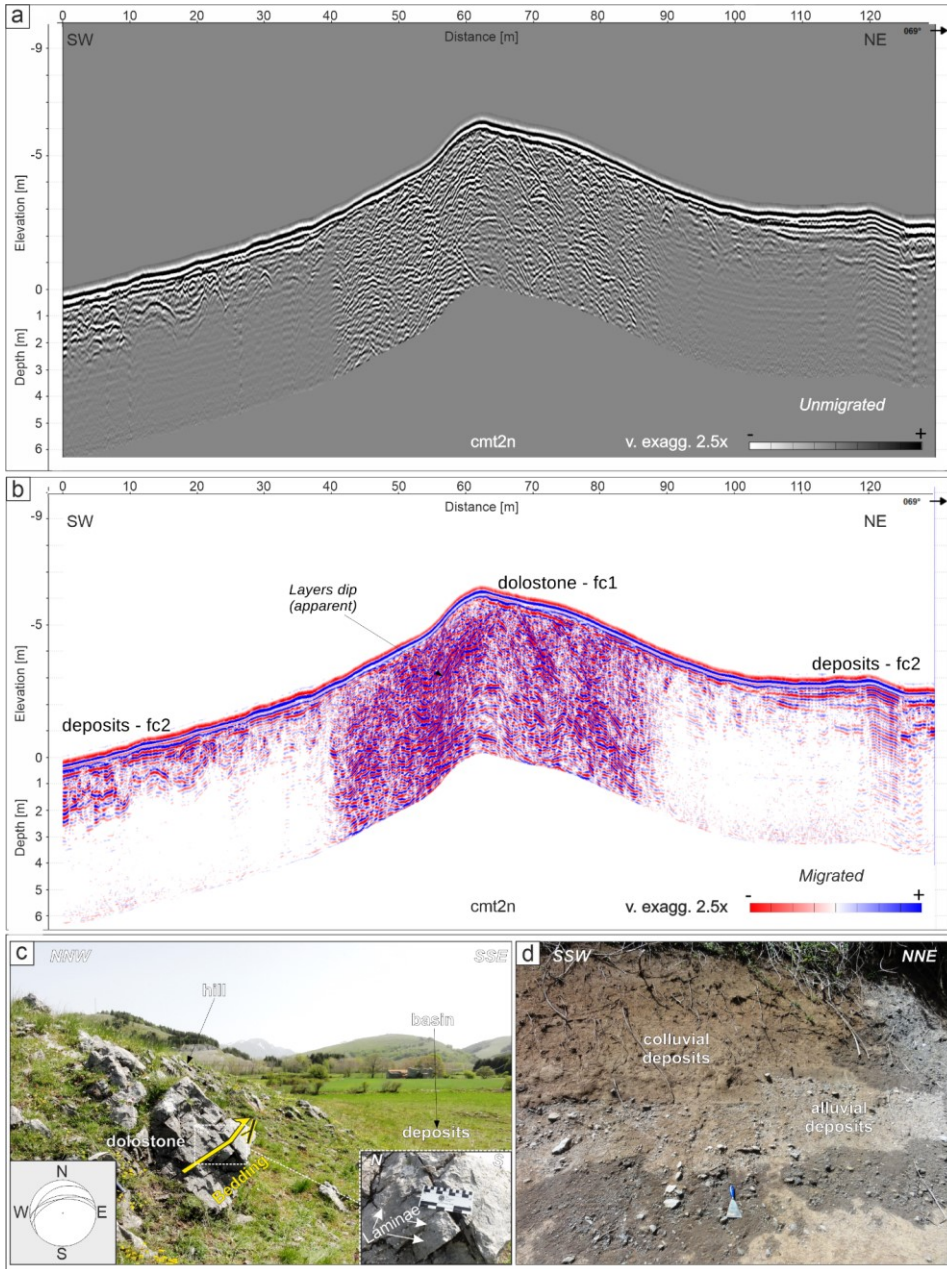


Figure 7

2

3

4

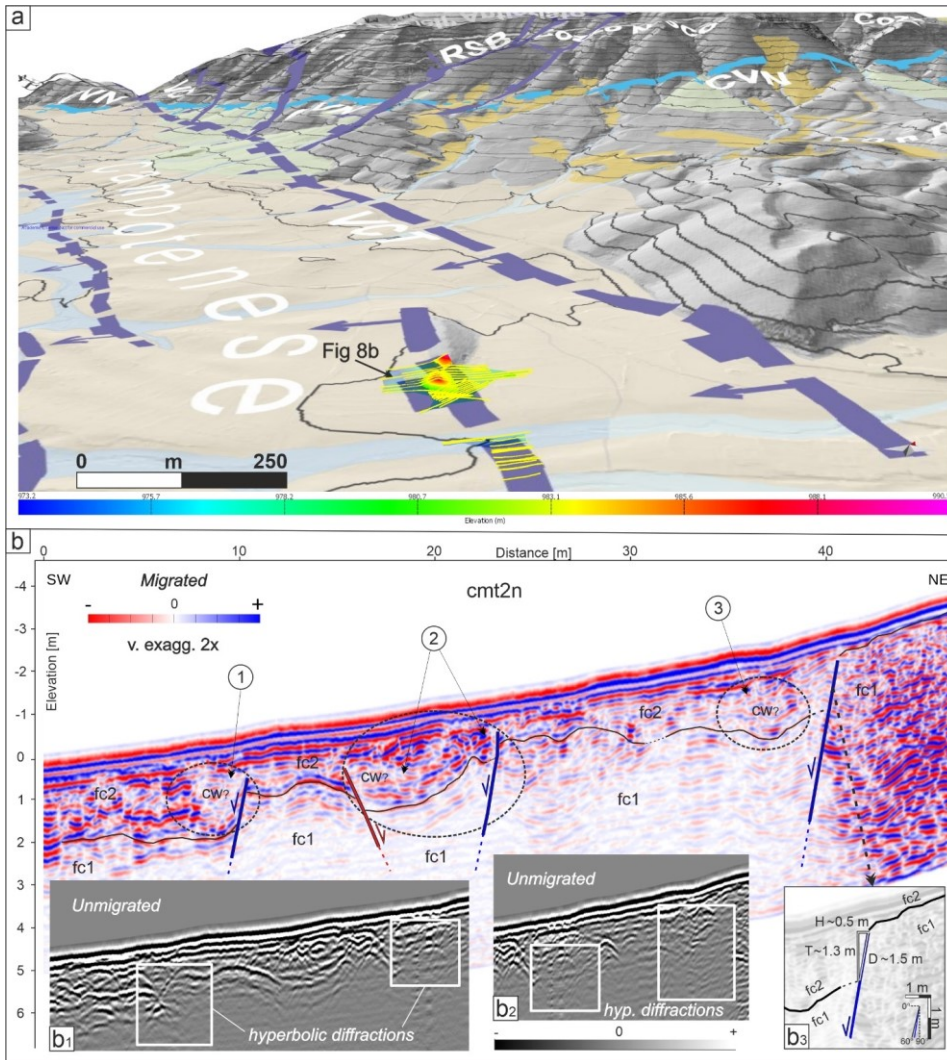


Figure 8

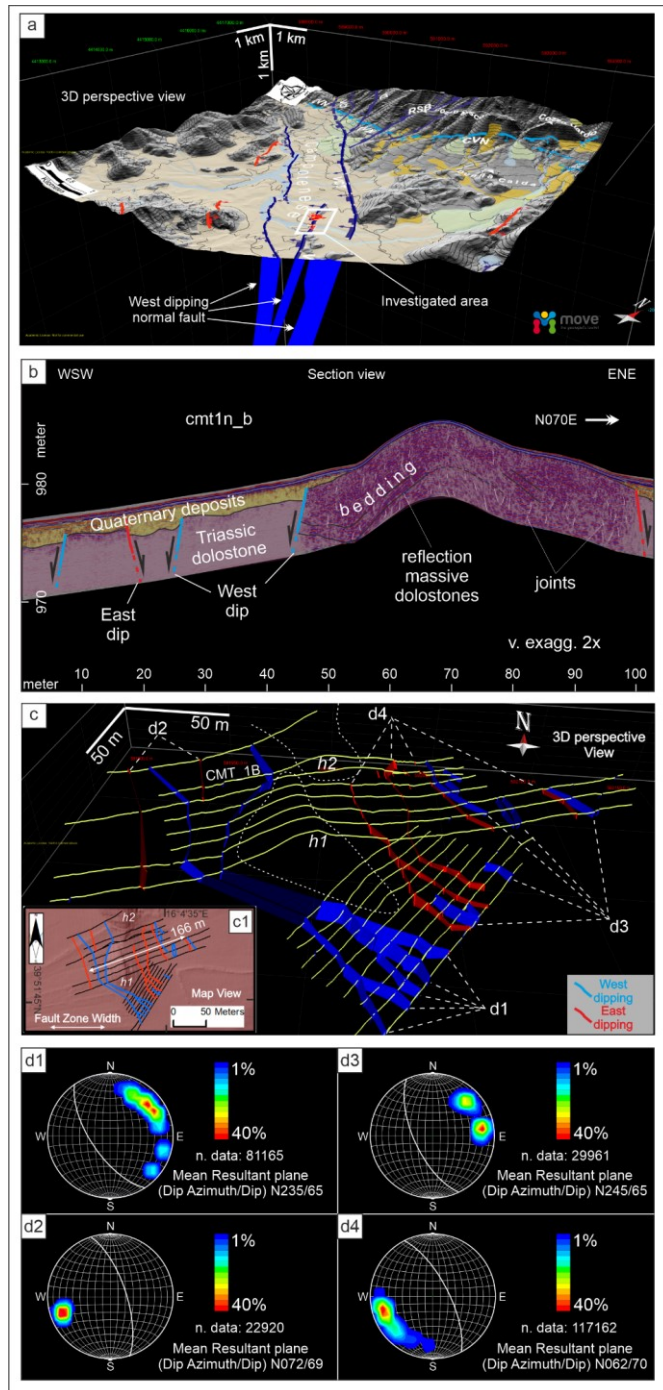


Figure 9

1

Table 1

GPR survey information and parameters		
Antenna frequency (MHz)	300 (preferred)	500
Number of acquired profiles	45	4
Total profile length (m)	3789.5/4153	363.5/4153
Profile distance (m)	10 and 25 (in g1 and g2)	not regular
Traces distance (m)	0.05	0.02
Number of samples	1024	512
Time window (ns)	300-200*	200-100*

2

3

Table 2

Processing Flow	Parameters (300 MHz)	Parameters (500 MHz)
Trace editing, coordinates editing and corrections	-	-
Time-zero correction	-	-
Dewow (ns)	10	5
Amplitude recovery function: $g(t)=(1+a*t)*e^{(b*t)}$	linear: 0.5 (2014) & 1.2 (2015) exponent: 0.15 (2014) & 0.6 (2015)	linear: 0.5 (2014) & 1.2 (2015) exponent: 0.15 (2014) & 0.6 (2015)
Velocity analysis	Diffraction hyperbola fittyng	Diffraction yperbola fitting
Background removal (ns)	Applied from 5 ns to end (computed on all the traces)	Applied from 5 ns to end (computed on all the traces)
Bandpass filter (MHz)	32/96/650/700	64/112/750/800
F-K filter	customized	customized
Time migration (2D Kirchhoff)	2D velocity models	2D velocity models
Topographic correction	GNSS/GIS Elevations	GNSS/GIS Elevations
Time-depth conversion (Quaternary deposits)	$v = 0,7 \text{ m/ns}$	$v = 0,7 \text{ m/ns}$

4

5

Figures and Tables captions:

Figure 1 - Location maps of the study site (DTM sources: TINITALY by Tarquini et al., 2012 and by Regione Calabria - www.regione.calabria.it, under license IODL 2.0. - <https://www.dat.gov.it/iodl/2.0/>): a) the image illustrates the southern Italian peninsula with the regional faults pattern and the historical strong earthquakes (Rovida et al. 2020); b) map showing the studied region with local faults (modified after Brozzetti et al. 2017a), and epicenters (stars) and focal mechanisms of the mainshocks of the 2012-2014 seismic sequence (Scognamiglio et al., 2006); c) location of the GPR survey area within the Campotenese Quaternary basin crossing the Fosso della Valle - Campotenese (VCT) fault.

Figure 2 - GPR acquisition campaigns: a) GPR profiles collected at the study site Campotenese ("cmt", where "n" and "s" stay for North and South, "h1" and "h2" indicate the two Dolostone hills outcropping in the basin) during the three field visits (aerial image source: Regione Calabria - www.regione.calabria.it, under license IODL 2.0. - <https://www.dat.gov.it/iodl/2.0/>); b) acquisition phase using the 300 and 500 MHz antennae (in the insert) and GNSS receivers used for accurate data positioning; c) GNSS base station set up during the fieldwork.

Figure 3: Topographic correction of GPR profiles: a) example of accuracy degradation of GNSS data, displaying an outlier both in map view and in topographic profile, on which the positioning error is considerable; b) GNSS coordinates and topographic profile after the correction; c) raw GPR section displaying high reflectivity in the central sector; d) example of full processed profile with topography displaying various reflection patterns encompassing dipping reflections and diffractions. Vertical exaggeration is 4.

Figure 4: Migration tests performed during the GPR data processing: a) unmigrated 2D GPR profile, 300 MHz antennae, displaying hyperbolic diffractions (white arrows); b) migrated profile using a constant velocity $v = 0.07$ m/ns, light-blue arrows indicate good diffractions collapse; c) migration output obtained with a constant velocity $v = 0.09$ m/ns, with dark-blue arrows suggesting good migration results (migration artefacts are shown by red arrows); d) migration results using a constant velocity $v = 0.11$ m/ns, with dark-blue arrows highlighting good hyperbolas collapse, particularly within the high reflective unit; red arrows highlight clear migration smiles.

Figure 5: Example of 2D time-migration of radar profiles: a) example of hyperbolic diffractions fitting used for 2D velocity model building; a constant velocity value (0.07 m/ns) was assumed in deeper no-diffraction areas for interpolation purposes; b) 2D time-migration results, highlighting the good performance of the process, which collapsed the hyperbolic diffractions (white arrows) and restored reliable reflection geometry.

Figure 6: GPR data visualization: a) fence diagram showing the three-dimensional location of some representative GPR profiles in the northern sector of the study site; b) bidimensional GPR profile (cmt3n, see figure 2a for location) displaying the central high reflective sector and dipping reflections across the hill; c) spatial variation of a 2D amplitude-frequency spectrum linked to variable physical properties of media along the profile cmt3n. Vertical exaggeration is 4.

Figure 7: Correlation between GPR profiles and outcropping geology at the study site: a) unmigrated 300 MHz profile (cmt2n, see fig. 2b for location) displaying numerous hyperbolic diffractions; b) migrated profile displaying the apparent dip associated to fractured dolostone formation (facies fc1) and Quaternary deposits in the attenuated sectors (GPR facies fc2); c) Quaternary deposits of the basin (on the background) surrounding the Triassic Dolostone formation outcropping on the hill h1. The yellow arrows indicate the bedding, such as the stereo-net (left-side inset); the right-side inset report a detail of the laminae visible on site and nearby; d) an example of Quaternary colluvial and alluvial deposits outcropping nearby the survey site. Vertical exaggeration is 2.5.

Figure 8: GPR data interpretation: a) three-dimensional image of the surveyed area (see fig. 1c for location), displaying the Dolostone outcrops (grey colour), Blue dashed lines are the VCT and RSB faults (fig. 1b), whilst the light blue is CVN fault. In yellow lines the GPR profiles; the coloured surface is the interpreted Dolostone top reflection (DTM source: Regione Calabria - www.regione.calabria.it, under license IODL 2.0. - <https://www.dat.gov.it/iodl/2.0/>); b) migrated radar profile with the main interpreted normal faults (blue and red are W- and E- dipping structures, respectively) as well as related sedimentary structures within the Quaternary deposits (unmigrated data in b1 and b2); the inset b3 is a schematic representation illustrating the methodology used for extraction of the GPR fault displacement (D: displacement; T: throw; H: heave). GPR facies fc2 shows semi-continuous and sub-horizontal reflections (Quaternary deposits) overlapping fc1 (Triassic Dolostone, black line is the "top"). In circle 1, reflections package thickening and truncation with localized attenuation, are likely interpretable as "colluvial-wedge-like" (cw?) features, or deposits from

Deleted: ¶
¶

Deleted: the detailed

Deleted: location of the three historical seismic events

Deleted: (stars)

Deleted: detailed

Deleted: a possible

Deleted: splay

Deleted: grids

Deleted: has been

Deleted: vs true layer

Deleted: (

Deleted: red

Deleted: s

Deleted:)

Deleted: Quaternary deposits of the basin

Deleted: bounding the basin and the surveyed hill

Deleted: The

Deleted: represents the interpolated horizon reconstructed after the picking of

Deleted: splays

Deleted: and

Deleted: detail of

Deleted: in the two grey inserts

Deleted: :

Deleted: 1)

Deleted: fc1,

Deleted: n

Deleted: lapping

Deleted: the

Deleted: lower boundary (

Deleted: top

Deleted: , black line above fc2

Deleted: ;

Deleted: , which

Deleted:

Deleted: suggest

Deleted: the presence of a

1 degradation of earthquake fault free-face nearby of the hanging-wall ($D \sim 0.6$ m). In circle 2, $fc2$ show more
2 discontinuous, from subparallel to wavy reflections package downlapping the lower top Dolostone; the
3 asymmetric, truncated reflections thickening is bounded by two conjugate normal fault strands (east dip $D \sim$
4 0.5 m, west-dip $D = 0.4$ m) displacing both $fc1$ and $fc2$. In circle 3, contorted reflections package with limited
5 continuity, displaying thickening, truncation and distributed attenuation, suggesting colluvial wedge deposits
6 close to the main fault zone ($D \sim 1.5$ m, inset b3). Vertical exaggeration is 2.

7 Figure 9: Results of the three-dimensional analysis and interpretation performed on the entire GPR dataset:
8 a) 3D structural model of the Campotenese basin updated after Brozzetti et al., 2017a (DTM sources:
9 TINITALY by Tarquini et al., 2012 and by Regione Calabria - www.regione.calabria.it, under license IODL
10 2.0. - <https://www.dati.gov.it/iodl/2.0/>); b) GPR section view (cmt1n-b) with interpretation including synthetic
11 and antithetic fault splays (blue= W-to SW-dip; red=E-to NE-dip, respectively); c) detailed structural scratch
12 of faults obtained by the analysis and correlation of interpreted fault slaps across the entire GPR dataset; the
13 inset c1 is a conventional structural map oriented to the North and reporting the same fault sets to highlight
14 the maximum width derived for the fault zone d) synthetic stereo-net plots of the fault planes in c), reporting
15 the mean Dip Azimuth / Dip angle extracted for the identified four main sets of discontinuities, with a Dip
16 Azimuth ranging between $N\ 235-245^\circ$ and $N\ 062-072^\circ$ for the W-dipping and E-dipping normal faults,
17 respectively. Vertical exaggeration is 2.

18 Table 1: Main information and GPR parameters used during the data collection (* the time window was
19 adapted depending on the surveyed area).

20 Table 2: Customized flow and details of the parameters used during the processing of the GPR dataset.

Deleted: close to
Deleted: a
Deleted: W-dip normal fault
Deleted: vertical offset
Deleted: ;
Deleted:)
Deleted: mode
Deleted: more
Deleted: (fc1)
Deleted: top boundary
Deleted: reflectors
Deleted: possible
Deleted: offset
Deleted: ;
Deleted: 3)
Deleted: lying above fc2
Deleted: a
Deleted: with a W-dip normal fault
Deleted: 0.8
Deleted: vertical offset
Deleted: inferred
Deleted: after the geological mapping at the scale of the basin
Deleted: for the west
Deleted: East